Local Coupled Equatorial Variability Versus Remote ENSO Forcing in an Intermediate Coupled Model of the Tropical Atlantic

Serena Illig, Boris Dewitte

Local Coupled Equatorial Variability versus Remote ENSO Forcing in an Intermediate Coupled Model of the Tropical Atlantic

SERENA ILLIG AND BORIS DEWITTE

LEGOS, Toulouse, France

(Manuscript received 23 February 2005, in final form 21 February 2006)

ABSTRACT

The relative roles played by the remote El Niño–Southern Oscillation (ENSO) forcing and the local air–sea interactions in the tropical Atlantic are investigated using an intermediate coupled model (ICM) of the tropical Atlantic. The oceanic component of the ICM consists of a six-baroclinic mode ocean model and a simple mixed layer model that has been validated from observations. The atmospheric component is a global atmospheric general circulation model developed at the University of California, Los Angeles (UCLA). In a forced context, the ICM realistically simulates both the sea surface temperature anomaly (SSTA) variability in the equatorial band, and the relaxation of the Atlantic northeast trade winds and the intensification of the equatorial westerlies in boreal spring that usually follows an El Niño event.

The results of coupled experiments with or without Pacific ENSO forcing and with or without explicit air–sea interactions in the equatorial Atlantic indicate that the background energy in the equatorial Atlantic is provided by ENSO. However, the time scale of the variability and the magnitude of some peculiar events cannot be explained solely by ENSO remote forcing. It is demonstrated that the peak of SSTA variability in the 1–3-yr band as observed in the equatorial Atlantic is due to the local air–sea interactions and is not a linear response to ENSO. Seasonal phase locking in boreal summer is also the result of the local coupling. The analysis of the intrinsic sustainable modes indicates that the Atlantic El Niño is qualitatively a noise-driven stable system. Such a system can produce coherent interdecadal variability that is not forced by the Pacific or extraequatorial variability. It is shown that when a simple slab mixed layer model is embedded into the system to simulate the northern tropical Atlantic (NTA) SST variability, the warming over NTA following El Niño events have characteristics (location and peak phase) that depend on air–sea interaction in the equatorial Atlantic. In the model, the interaction between the equatorial mode and NTA can produce a dipolelike structure of the SSTA variability that evolves at a decadal time scale. The results herein illustrate the complexity of the tropical Atlantic ocean–atmosphere system, whose predictability jointly depends on ENSO and the connections between the Atlantic modes of variability.

1. Introduction

The last 15 yr have witnessed a tremendous improvement of our knowledge of the El Niño phenomenon. This, in particular, has been illustrated by the large effort of many research centers in the world for providing seasonal forecasts [see, e.g., the International Research Institute for Climate and Society (IRI) ENSO update and forecasts, online at http://iri.columbia.edu/climate/ENSO/currentinfo/SST_table.html]. These forecasts are not only useful for assessing socioeconomic impacts in surrounding regions of the Pacific Ocean, but also in regions far from the Pacific Ocean. The availability of such diagnostics and their interpretation has also highlighted the need to improve our understanding of the ENSO teleconnections and the inherent variability of the remote regions influenced by ENSO. Of particular interest is the tropical Atlantic whose oceanic variability impacts not only the African climate (Janicot et al. 1998; Fontaine and Janicot 1999) but also northern Europe (Cassou and Terray 2001; Drévillon et al. 2003).

The tropical Atlantic is a region of significant climate fluctuations at various time scales whose links with ENSO have not been completely elucidated (see Xie and Carton 2004 for a review) at a time when seasonal forecasts in that region are becoming an urgent economic and scientific challenge (Chang et al. 2003). At interannual time scales, two main modes emerge from observational studies: the meridional or dipole mode (Weare 1977; Servain 1991; Nobre and Shukla 1996;

Corresponding author address: Serena Illig, LEGOS, 14 av. E. Belin, 31400 Toulouse, France.
E-mail: illig@notos.cst.cnes.fr

Chang et al. 1997; Servain et al. 1999; Servain et al. 2000; Sutton et al. 2000) and the equatorial mode (Merle et al. 1980; Hisard 1980; Philander 1986). Whereas the dynamics and forcing of the meridional mode remain ambiguous (Houghton and Tourre 1992; Enfield and Mayer 1997), the equatorial mode is likely the result of ocean–atmosphere coupling similar to the Pacific ENSO mode, as pointed out by Zebiak (1993, hereafter Z93).

Following the early work of Z93, there have been a lot of modeling efforts to delineate the ENSO effects on these two modes from "tools" of various complexities. Latif and Barnett (1995), and more recently Nobre et al. (2003), used an ocean general circulation model (OGCM) coupled to a statistical atmosphere to address the issue of the tropical teleconnections over the tropical Atlantic. Although they benefit from a better representation of the oceanic circulation in comparison to Z93, the use of a statistical atmosphere to predict surface wind stress anomalies over the tropical Atlantic is a limitation considering the highly nonlinear teleconnection processes. This leads to an overestimation of the local ocean–atmosphere coupling and an underestimation of the remote influence of ENSO. Delecluse et al. (1994) and Saravanan and Chang (2000) emphasized the significant contribution and the complex nature of the teleconnections between the tropical Pacific and Atlantic using an atmospheric general circulation model (AGCM) forced with different SST fields. However, forced experiments (as opposed to coupled ones) remain difficult to interpret in regions where air–sea feedbacks contribute as much to SSTA variability as remote forcing. Recently, Huang (2004) proposed a comprehensive model setting for investigating the remotely forced variability in the tropical Atlantic Ocean. From the analysis of an ensemble simulation of a state-of-the-art ocean–atmosphere general circulation model fully coupled only within the Atlantic basin, he concludes that the ENSO influence modulates the temporal fluctuations of the intrinsic patterns of the tropical Atlantic instead of generating distinctive new ones. This calls for more investigations of the dynamical responses of the equatorial Atlantic (EA) to flux anomalies associated with changes in the Walker circulation.

In the study, we present a tropical coupled model of intermediate complexity that is used to 1) document the dynamics of the so-called Atlantic El Niño mode, and 2) to investigate the remote impact of ENSO over the tropical Atlantic sector and the role of the equatorial mode on the simulated teleconnection pattern. We concentrate on the equatorial mode and rather than a priori considering that it passively undergoes the remote forcing, we question the extent to which it is involved in the dynamical adjustment of the response of the tropical Atlantic variability to ENSO. From a methodological point of view, our goal is to avoid the relative heaviness of a full coupled general circulation model (CGCM) that still exhibits drifts and biases in the mean state and seasonal cycle (AchutaRao et al. 2004), despite its comprehensive physics. Here, we therefore design an anomaly model so that simulated interannual variability is always relative to a realistic prescribed climatology. Such a modeling approach allows for numerous tests and also eases the interpretation. Because our focus is on equatorial wave dynamics and the associated coupled response, we chose a linear model for the oceanic component of the coupled model. This is also motivated by a recent study by Illig et al. (2004, hereafter ID04) that showed that equatorial waves contribute significantly to the sea level and surface current variability in the EA. In particular, linear theory can be used to depict the oceanic EA variability with similar skill to the tropical Pacific, as long as the baroclinic mode energy distribution based on realistic density profiles is taken into account. Thus, we extend the Z93 study by considering a more realistic background state of the ocean. Note that the consideration of several baroclinic modes in the oceanic component of the coupled model is also likely to impact the model coupled variability as was found in the Pacific by Dewitte (2000). This can support the interpretation of the dominant time scales of the variability in the tropical Atlantic. Moreover, seasonally varying mean states (mean currents, mixed layer depth) are taken into account in the sea surface temperature anomaly (SSTA) formulation. This enriches the spectrum of the variability through the nonlinear interactions between the seasonal cycle and simulated interannual modes. Finally, we use a global AGCM that allows the prescription of observed ENSO forcing in the Pacific sector and explicitly treats the ENSO tropical teleconnections, conversely to Z93.

This paper is organized as follows. In section 2 we present the various datasets and the coupled model. Various aspects of the model variability, including ENSO teleconnections, are validated from the observations for both components in a forced context. Section 3 investigates the nature of the coupled mode in the tropical Atlantic that can be sustained within a realistic parameter range and discusses the preferred time scales of the variability from interannual to decadal. The stability of the simulated equatorial mode is estimated. Section 4 analyzes the results of various experiments where the interannual SST forcing is restricted to specific regions. The role of the local coupling both in the equatorial and the northern tropical Atlantic

(NTA) are estimated for the 1982–2001 period. Section 5 provides a discussion of the results presented in this paper, followed by conclusions.

2. Data and model description

a. Data

1) ERA-40

Monthly mean wind stress and heat flux (latent, sensible, short- and longwave) from the European Centre for Medium Range Weather Forecasts (ECMWF) 40-yr Re-Analysis (ERA-40) project are used. ERA-40 is a global atmospheric analysis of many conventional observations and satellite data streams for the period of September 1957 through August 2002. We interpolated these datasets to the model grids using a bilinear interpolation (original resolution is 2.5° × 2.5°).

2) REYNOLDS SST

The Reynolds monthly sea surface temperature (SST) fields combine in situ and satellite data using optimum interpolation (version 2) from 1982 to 2003 on a 1° × 1° spatial grid (Reynolds and Smith 1994) and use EOF reconstruction from 1950 to 1981 on a 2° × 2° spatial grid (Smith et al. 1996). We merged these datasets into a continuous SST field on a 1.875° latitude × 4° longitude grid (the atmospheric model grid) using a bilinear interpolation.

3) TAOSTA

Vauclair and du Penhoat (2001) have collected near-surface and subsurface in situ temperature observations of the tropical Atlantic Ocean between 1979 and 1998, and have built surface and subsurface bimonthly temperature fields [the Tropical Atlantic Ocean Subsurface Temperature Atlas (TAOSTA), available online at http://medias.obs-mip.fr/taosta/]. The interpolation is based on an objective analysis (Bretherton et al. 1976) and provides a gridded dataset from 30°S to 30°N and from 70°W to 12°E on a 2° × 2° spatial grid with 14 vertical levels (same as those of Levitus et al. 1998).

4) MIXED LAYER DEPTH

Global mixed layer depth (MLD) climatology from de Boyer Montégut et al. (2004) is estimated using in situ temperature profiles, for which the MLDs are estimated using a difference criterion of 0.2°C between the surface reference depth (10 m) and the base of the mixed layer. A gridded product is then built on a 2° × 2° spatial grid every month.

In the following, seasonal cycles are computed over the 1982–2001 period, and interannual anomalies are estimated with respect to these seasonal cycles. The significance level of the correlation is estimated as in Sciremammano (1979). The fast Fourier transform (FFT) analysis significance levels are estimated assuming a chi-squared distribution with 2 degrees of freedom of the FFT power spectrum. The Morlet wavelet is used for the time–frequency analysis. The computational procedure of the wavelet analysis is described by Torrence and Compo (1998).

b. The coupled model: TIMACS

In this section, we present the Tropical Intermediate Model for Atlantic Climate Studies (TIMACS). TIMACS is composed of an atmospheric model that uses global SST to forecast wind stress anomalies (TXA and TYA) and net heat flux anomalies (QnetA). This atmosphere is coupled in the EA to an anomalous ocean model. Outside EA, boundary conditions derived from observations are prescribed.

1) ATMOSPHERIC COMPONENT: QTCM

The atmospheric component is the quasi-equilibrium tropical circulation model (QTCM) from Neelin and Zeng (2000) and Zeng et al. (2000). This model is based on the quasi-equilibrium approximations in the convective parameterization. It includes a single deep convective mode in the thermodynamic vertical structure and two components (baroclinic and barotropic) in the velocity vertical structure. We have used the standard version of this intermediate complexity atmospheric model, QTCM1 version 2.3 (available online at http://www.atmos.ucla.edu/~csi/QTCM), except that we have defined a higher-resolution grid mesh in the latitudinal direction, in particular, to account for the fact that the tropical Atlantic SSTAs are narrowly confined to the equatorial region. Thus, the horizontal resolution is 1.875° × 4° instead of 3.75° × 5.625°. For numeric stability considerations, the viscosity parameter was adjusted to 5×10^5 m^2 s^{-1} (instead of 7×10^5 m^2 s^{-1} in the standard resolution version).

A control run QTCM experiment forced by the Reynolds SST from 1982 to 2001 is performed (hereafter QTCM-CR). The spinup is achieved by forcing the model using the monthly mean of Reynolds SST from early 1976 to the end of 1981. The model skill is assessed through a comparison with the ERA-40 reanalysis. Figure 1 presents the correlation and the variability of the simulated field for zonal wind stress (TXA) and QnetA monthly anomalies. QTCM wind stress formulation calls for standard bulk formula using a drag co-

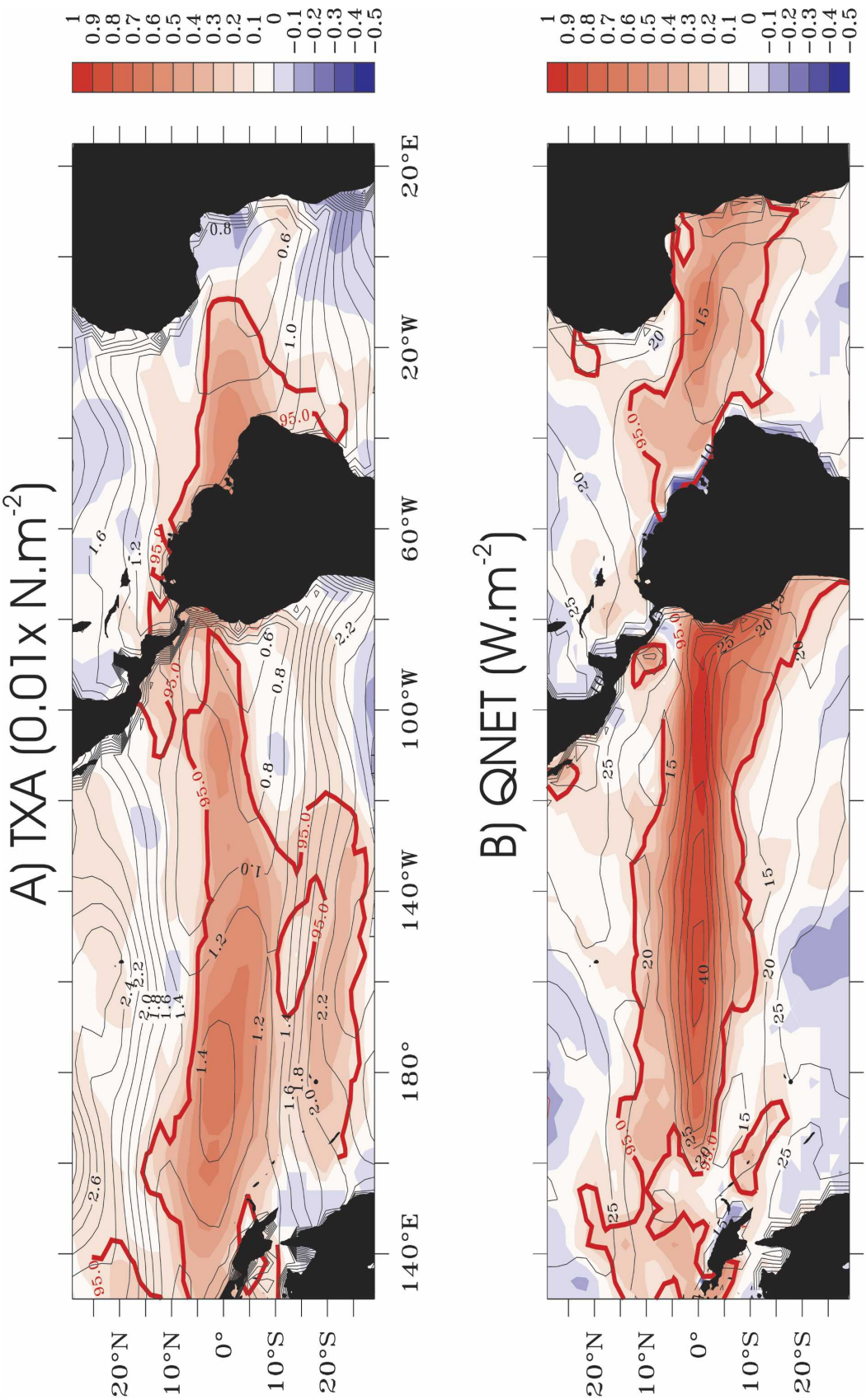

FIG. 1. Comparison between QTCM-CR and ERA-40 over the tropical Pacific–Atlantic sector over the 1982–2001 period. (a) TXA (0.01 N m^{-2}) and (b) QnetA (W m^{-2}) correlation between model and observations is shaded and the model variability is contoured. The red thick line indicates the 95% level of significance of the correlation.

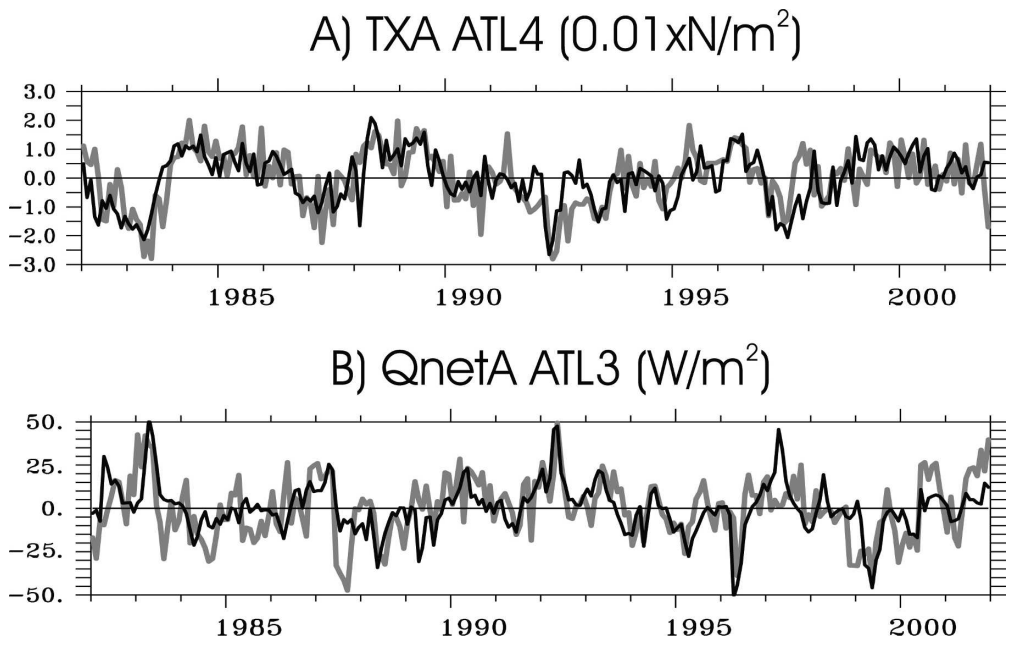

FIG. 2. Comparison between QTCM-CR outputs and ERA-40 in the tropical Atlantic over the 1982–2001 period: QTCM (black line) and ERA-40 (gray line) (a) ATL4 (0.01 N m^{-2}) and (b) QnetA ATL3 (W m^{-2}).

efficient value of 1.375×10^{-3}. QnetA is the sum of the radiative (short- and longwave heat fluxes) and turbulent flux (latent and sensible heat fluxes) anomalies, computed using a radiation scheme and bulk formula, respectively (see Zeng et al. 2000 for details). Not surprisingly, the best fit between observations and the simulation is found in the 10°S–10°N equatorial belt where the deep convection is usually observed. The correlation between QTCM-CR and ERA-40 is largely significant at a 95% level of confidence over most of the equatorial Pacific and Atlantic. In particular, in the tropical Pacific (Atlantic) wind forcing region (Fig. 1a), the correlation between modeled and observed TXA peaks at values larger than 0.6 (0.5). Note that comparable values were obtained with the coarser-resolution version of the model (slightly lower in the EA). It is worth pointing out that the root-mean-square (rms) differences between QTCM and ERA-40 are always lower than the variability of the signal in the equatorial band (not shown). Note also that applying a 3-month running mean on the time series results in an increase by $\sim +0.15$ of the correlation between ERA-40 and QTCM-CR TXA.

Based on the wind-forcing region highlighted in Fig. 1, we define a new index, ATL4, as the area-averaged TXA over (3°S–3°N, 50°–25°W) (cf. Fig. 7c). The simulated and observed TXA ATL4 time series are shown in Fig. 2a. Both time series exhibit a coherent timing sequence of intensification and reduction of the trade winds, with comparable magnitudes. This index highlights an important interannual variability, with a foremost low frequency (3–6 yr), together with contributions from near-annual and intraseasonal time scales. The observed and simulated indices have a level of correlation of 0.6, while the rms difference does not exceed 0.84×10^{-2} N m^{-2}. The frequency analysis of these indices (not shown) confirms that QTCM reproduces well the observed low frequencies (>3 yr) as well as the higher frequencies (1–3 yr).

Figure 2b shows the results of the comparison between the modeled and the observed heat flux for the ATL3 (3°S–3°N, 20°W–0°) index. The QTCM QnetAs are in good agreement with the observations in the region of significant QnetA variability, which also corresponds to the region of large SSTA variability. The correlation peaks at 0.57 in the ATL3 region, and the rms difference is lower than 15 W m^{-2}. These results should be taken with caution considering the energetic unbalance at the air–sea interface in the case of forced experiments. Note, however, that increasing the resolution in QTCM significantly "improves" the simulation of the net heat fluxes anomalies in the tropical Atlantic with a correlation (rms difference) increased (decreased) by 20% (7%) in ATL3. Overall, although the ENSO teleconnection pattern in the tropical low-tropospheric circulation is somewhat less pronounced over the tropical Pacific than in the standard version of QTCM, the high-resolution version of the model leads

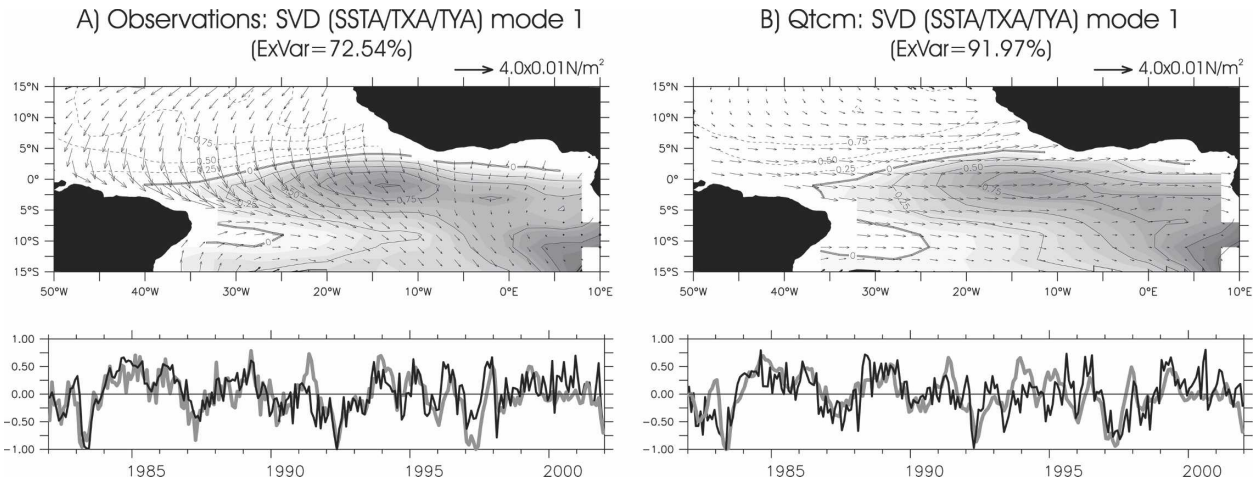

FIG. 3. Dominant mode of the results of the SVD between SSTA and wind stress anomalies over the 1982–2001 period, for (a) the observations and (b) QTCM-CR. (top) The spatial structures of the SSTA are shaded every 0.1°C and contoured every 0.25°C. The wind stress anomalies are represented with arrows (scale in the top-right corner, units are 0.01 N m^{-2}). (bottom) The associated normalized time series are represented in gray line for the SSTA and black line for wind stress. The time series of SSTA and wind stress anomalies are correlated with a 0.66 level for the observations and a 0.57 level for QTCM-CR. The percentage of covariance explained by the mode is indicated on top of each plot.

to an improved simulation of some meteorological fields, in particular the outgoing longwave radiation and the zonal wind stress, both in terms of interannual variability and propagation characteristics (D. Gushchina 2005, personal communication).

To highlight the coupled variability in the tropical Atlantic, a multivariate singular value decomposition (SVD) analysis between wind stress and SST anomalies is performed for both observations and the QTCM-CR outputs. The results are displayed in Fig. 3, which confirms the good agreement between observed and simulated SST-associated wind stress anomalies, particularly in the western part of the EA. The percentage of explained variance and correlation between the time series of wind stress and SST anomalies of the SVD mode are comparable for the model and observations. The most prominent flaw of the model is associated with a zonal wind flow that extends the variability of the equatorial trade winds too much to the east. This is associated with an underestimation of the simulated meridional wind stress anomalies in the model. Such bias of the model, in particular in the eastern Atlantic, may lead to unrealistic forcing of Kelvin and Rossby waves in the eastern part of the basin, which will lead to the definition of a limited coupling zone [see section 2b(4)].

ENSO teleconnections

In addition to its computational cost effectiveness, the use of QTCM was motivated by recent studies indicating that the model is not only useful for investigating ENSO teleconnection mechanisms (Su and Neelin 2002; Su et al. 2001; Neelin et al. 2003; Neelin and Su 2005), but that its skill is comparable to full AGCMs (Zeng et al. 2000; Gushchina and Dewitte 2005). It also simulates an internal variability whose spatiotemporal characteristics are as realistic as other AGCMs (Lin et al. 2000), which is important in the modeling framework presented here.

As an illustration of the model skill in simulating ENSO teleconnections over the tropical Atlantic sector, we follow the recent observational study by Czaja et al. (2002) and carry out the following diagnostic on the model outputs: the zonally averaged (40°–20°W) wind stress anomalies and QnetA are regressed on the December–January–February (DJF) average of the Reynolds Niño-3 SST index defined as the SST anomalies averaged over (5°S–5°N, 150°–90°W) for the 1982–2001 period. The results for QTCM and ERA-40 are displayed in Fig. 4. Consistent with results of Czaja et al. (2002, their Fig. 5), Fig. 4a indicates that most ENSO events are associated with a northward shift of the spring intertropical convergence zone (ITCZ)—south of 5°N, we observe a strengthening of the southeast trade winds associated with negative SSTA in the equatorial belt. This cooling, associated with positive heat flux anomalies, is intensified in May–June when the equatorial upwelling is maximum, consistent with the results of observational studies (Enfield and Mayer 1997; Klein et al. 1999; Vauclair et du Penhoat 2001). Further north, we observe a weakening of the northeast trade winds from January to March, which leads to a

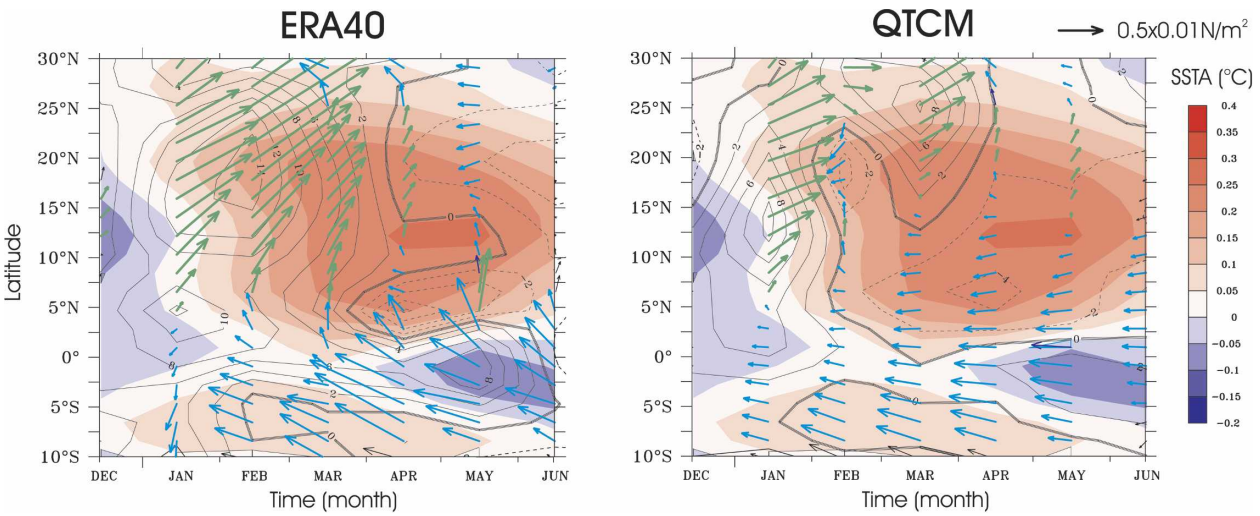

FIG. 4. Regression map of the surface wind stress (blue arrows for positive and green arrows for negative TXA, scale in the top-right corner), QnetA (contoured every 2 W m^{-2}, positive into the ocean, dashed when negative, zero contour thickened), and SSTA (shaded, °C) onto the Niño-3 SSTA index in DJF (normalized by its variability) for (left) ERA-40 and (right) QTCM.

reduction in evaporation and positive QnetA toward the ocean, on the order of 5–10 W m^{-2}. It induces a warming of the SSTA around March–April–May (MAM) of about 0.5°C between 5° and 25°N. After April, the trade wind anomalies disappear, and the SSTA decreases through evaporation losses.

For QTCM, despite the fact that the shift of the ITCZ is too far north and that the northeast trade wind relaxation is less intense and briefer, the main features of the ENSO remote influence on the tropical Atlantic are well reproduced. Note again that the meridional wind stress variability associated with the ENSO teleconnections is too weak for the model as compared to the observations. The reader can also refer to Su et al. (2001), Neelin et al. (2003), Gushchina and Dewitte (2005), and Neelin and Su (2005) for evaluating the model performances in reproducing ENSO teleconnections.

QTCM exhibits relatively good performance in simulating the atmospheric response to ENSO over the tropical Atlantic, especially in the equatorial band. Nevertheless, the response of the NTA is less consistent with the observations. This could be due to numerous reasons. First, because of air–sea feedback in that region (Klein et al. 1999; Czaja et al. 2002), the interpretation of a locally forced simulation is ambiguous. This is because the SST forcing already contains the atmospheric response to ENSO. Running QTCM without local interannual forcing in the tropical Atlantic (boundary conditions in the tropical Atlantic are only seasonal SST) leads to a more realistic relaxation of the northeast trade winds in January–February–March (not shown). After March, however, there is no wind or heat flux reversal through evaporation in this simulation. This emphasizes that these are local responses to SST. Second, simulated meridional wind stress variability is unrealistically weak, which tends to spread the atmospheric circulation in the zonal direction. This is a flaw of most forced AGCMs, which may contribute to the lack of skill in simulating the ENSO teleconnection in this region where the ITCZ migrates seasonally.

With these model characteristics in mind, we will focus on the equatorial teleconnections (10°S–10°N). We assume that the mechanisms leading to the equatorial response to ENSO in QTCM, if connected to the NTA variability, are sufficiently realistic. This will be discussed in the final section.

2) OCEAN COMPONENT: OLM

The tropical Atlantic Ocean component is an ocean linear model (OLM), similar to that of Cane and Patton (1984), but with a higher resolution and more realistic coastlines (see ID04). The model domain extends from 28.875°S to 28.875°N, and 50°W to 10°E, with a horizontal resolution of 0.25° in latitude and 2° in longitude. The model time step is 2 days. It includes six baroclinic modes with phase speed c_n, projection coefficient P_n, and friction r_n, derived from a high-resolution OGCM simulation forced with realistic fluxes (Barnier et al. 2000). This OGCM simulation will be referred to as the CLIPPER dataset hereafter. The results of the linear model forced with realistic winds were compared to various observations and to CLIPPER in ID04. The

reader is referred to this latter paper for more details on the skill of the OLM in a forced context.

A mixed layer model (MLM) is embedded in the ocean model that consists of a thermodynamical budget in a surface layer whose thickness $\overline{h}_{\mathrm{mix}}$ depends on both space and season. The horizontal resolution is 1° in latitude and 2° in longitude and the time step is 1 day. The equation for the SST anomaly is similar to the one used in Zebiak and Cane (1987), but with a different parameterization of the subsurface temperature T_{sub} (see below), and different climatological surface currents, upwelling, and SST. Also, the actual heat flux derived from the bulk formulas is used, as opposed to the heat flux parameterization used by Zebiak and Cane (1987) and Z93. The thermodynamic equation has the following form (barred quantities represent seasonal fields and unbarred quantities represent interannual anomalies relative to the seasonal cycle):

$$\partial_t T = \begin{cases} \text{zonal advection} \begin{cases} -u\partial_x(\overline{T}+T) & \text{(a)} \\ -\overline{u}\partial_x(T) & \text{(b)} \end{cases} \\ \text{meridional advection} \begin{cases} -v\partial_y(\overline{T}+T) & \text{(c)} \\ -\overline{v}\partial_y(T) & \text{(d)} \end{cases} \\ \text{vertical advection} \begin{cases} -[M(\overline{w}+w)-M(\overline{w})]\partial_z\overline{T} & \text{(e)} \\ -M(\overline{w}+w)\partial_z T & \text{(f)} \end{cases} \\ \text{and heat fluxes,} \quad +\dfrac{(Q_{\mathrm{net}}+Q_c)}{\rho C_p \overline{h}_{\mathrm{mix}}} \quad \text{(g).} \end{cases} \quad \text{(Eq. 1)}$$

The prescribed seasonal surface currents $\overline{u}$, $\overline{v}$, and $\overline{w}$ are obtained by forcing the OLM with the ERA-40 climatological wind stresses. The main characteristics of these climatological current are presented and compared to the observations and CLIPPER in the appendix B. The specified seasonal cycle of SST ($\overline{T}$) is derived from the Reynolds SST (Reynolds and Smith 1994) over the 1982–2001 period.

The mean vertical temperature gradient $\overline{T}_z$, in term (5), is defined from a seasonally varying MLD, $\overline{h}_{\mathrm{mix}} = \overline{h}_{\mathrm{mix}}(x, y, t_{12})$. The latter is prescribed from de Boyer Montégut et al. (2004).

Here $M(x)$ is a step function defined by $M(x) = \begin{cases} 0, & x \le 0 \\ x, & x > 0 \end{cases}$. This function accounts for the fact that SSTAs are affected by vertical advection only in the presence of upwelling.

The anomalous vertical temperature gradient $\partial_z T$ is defined as $\partial_z T = (T - T_{\mathrm{sub}})/\overline{h}_{\mathrm{mix}}$, where T_{sub} is the temperature anomaly at the base of the mixed layer. A new parameterization for the temperature anomalies at the base of the mixed layer is proposed that depends explicitly on the baroclinic mode contribution to pressure anomaly and the local stratification. With $p(x, y, z, t) = \Sigma_{n=1}^{M} p_n(x, y, t) \times F_n(z)$, where p is the pressure field, $p_n(x, y, t)$ is the associated n baroclinic mode contribution and F_n is the vertical structure of the nth baroclinic mode derived from the CLIPPER stratification at 14°W. The hydrostatic relation leads to $\delta\rho = \rho_0 \Sigma_{n=1}^{M} \mathrm{sl}_n \times \partial_z[F_n(z)]$, where ρ is the density and sl_n is the n baroclinic mode contribution to sea level anomalies ($\mathrm{sl}_n = p_n/\rho_0 g$). Using the stability equation for the density field and assuming that the density changes (at constant depth) are governed by temperature changes [i.e., $\delta\rho = \rho\alpha_T\delta T$, with $\alpha_T = 2.97 \times 10^{-4}\ \mathrm{K}^{-1}$ (Gill 1982)], the anomalous vertical temperature gradient ($\rho_0\rho^{-1} \approx 1$) can be written as

$$T_z(x, y) = \frac{T(x, y) - \alpha_T^{-1} \sum_{n=1}^{6} \mathrm{sl}_n(x, y, t) \times \partial_z\{F_n[\max(\overline{h}_{\mathrm{mix}}, 50\ \mathrm{m})]\}}{\overline{h}_{\mathrm{mix}}}.$$

Note that near the surface a large number of baroclinic modes are required to correctly represent the density field and to account for the small vertical scales in the variability. Retaining the six gravest baroclinic modes is sufficient to represent the temperature variability below the first 50 m (see appendix A).

Unlike Zebiak and Cane (1987), anomalous heat fluxes are not parameterized with a temperature-damping term, but are derived from the bulk formulas embedded in the atmospheric component. Moreover, a corrective flux term (Q_c) was added in order to compensate for a systematic cold bias (of the order of ~ -0.05°C in the ATL3 region) found in an earlier version of the model run. This cold bias is due to enhanced climatological vertical advection of anomalous temperature when the system is run in a coupled mode. Rather than arbitrarily reducing mean upwelling, we choose to apply this statistical heat flux correction derived from the mean SSTA pattern of a 100-yr coupled run without correction. It is assumed that this term does not drastically modify the model physics. This was checked on some of the analyses performed in this

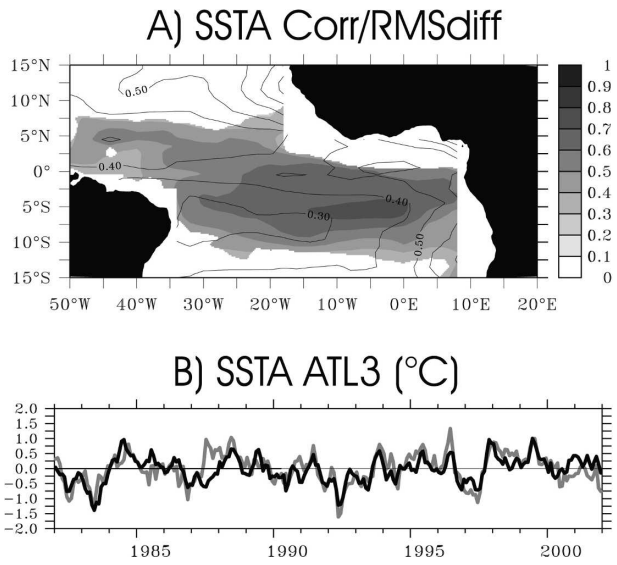

FIG. 5. (a) Comparison between the OLM-CR and the Reynolds SSTA in the tropical Atlantic over the 1982–2001 period. The correlation significant at a 95% level (rms difference) is shaded (contoured). (b) OLM-CR (black line) and Reynolds (gray line) ATL3 index. Unit: °C.

study (in particular on the SVD modes between wind stress and SST anomalies).

A control experiment in a forced context is performed to validate simulated SST anomalies (hereafter OLM-CR). The forced context is achieved in the following manner: the ocean model is forced by the ERA-40 wind stress anomalies over the OLM domain from 1982 to 2001. In the tropical Atlantic sector, the atmospheric component is forced by the sum of the MLM SSTA and the Reynolds SST climatology. Elsewhere, the Reynolds SST is prescribed. The heat flux anomalies required to force the MLM are obtained by retrieving, at each MLM time step, the heat flux seasonal cycle from the daily averaged QTCM heat fluxes. The latter was computed from a QTCM run forced by seasonal SST. The spinup is realized by forcing QTCM for 4 yr (1976–79) by the Reynolds SST climatology over the globe, while the OLM is forced by ERA-40 wind stress anomalies (MLM fluxes being parameterized with a damping term). From January 1980, QTCM is forced in the tropical Atlantic by the MLM SSTA. From January 1981, the MLM is forced by heat flux anomalies simulated by QTCM. Results are analyzed for the January 1982–December 2001 period.

Figure 5a displays the correlation and rms difference between the simulated SSTA and the Reynolds SSTA. The simulated SSTA is in good agreement with the observations; in the 10°S–10°N equatorial belt, the correlation is largely significant (with a level of confidence of 95%) and the rms difference does not exceed 0.6°C. In Fig. 5b, the ATL3 index is plotted for the model and the observations. Both time series exhibit a coherent sequence of warm and cold events, with similar magnitudes: the correlation (rms difference) of these time series reaches 0.71 (0.36°C). A multivariate SVD analysis is performed with the OLM-CR SSTA and the wind stress anomalies from ERA-40. The results are displayed in Fig. 6. As in the observations (Fig. 3a), westerlies in the western EA are associated with SST anomalies in the central basin that reach 1.25°C. This mode explains 75% of the covariance close to the observations. As expected from equatorial wave dynamics, the variability is more confined toward the equator with less extension to the south than in the observations. Compared to observations, the peak variability along the equator is too far to the west. This may reflect an overestimation of the western boundary reflection in the model. Note, however, the realistic location of the zero line north of the equator for SST anomalies, which has to be related to the appropriate representation of the oceanic model vertical structure (see ID04). Overall, the dominant characteristics of the equatorial mode are correctly simulated, which is encouraging for carrying fully coupled experiments.

3) COUPLING STRATEGY

The coupling strategy is based on the principle that, given the relative simplicity of the system, air–sea coupling should takes place where the model exhibits the best skill. Therefore, coupling zones have been defined. They correspond to the region of correlation significant

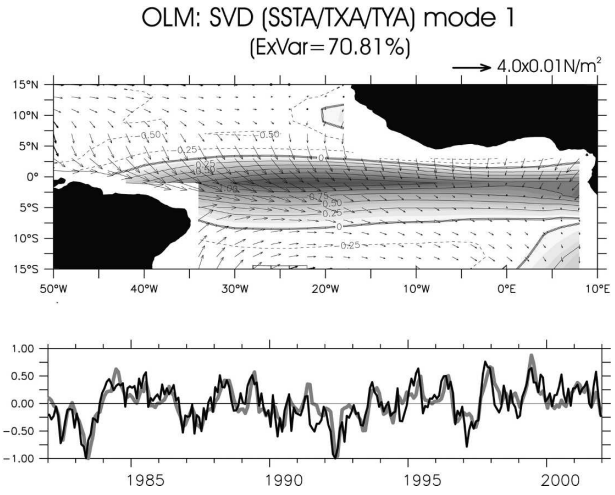

FIG. 6. Same as Fig. 3, but for the oceanic component of the TIMACS model forced by ERA-40 wind stress anomalies (OLM-CR). The normalized time series of SSTA and wind stress anomalies are correlated with a 0.79 level.

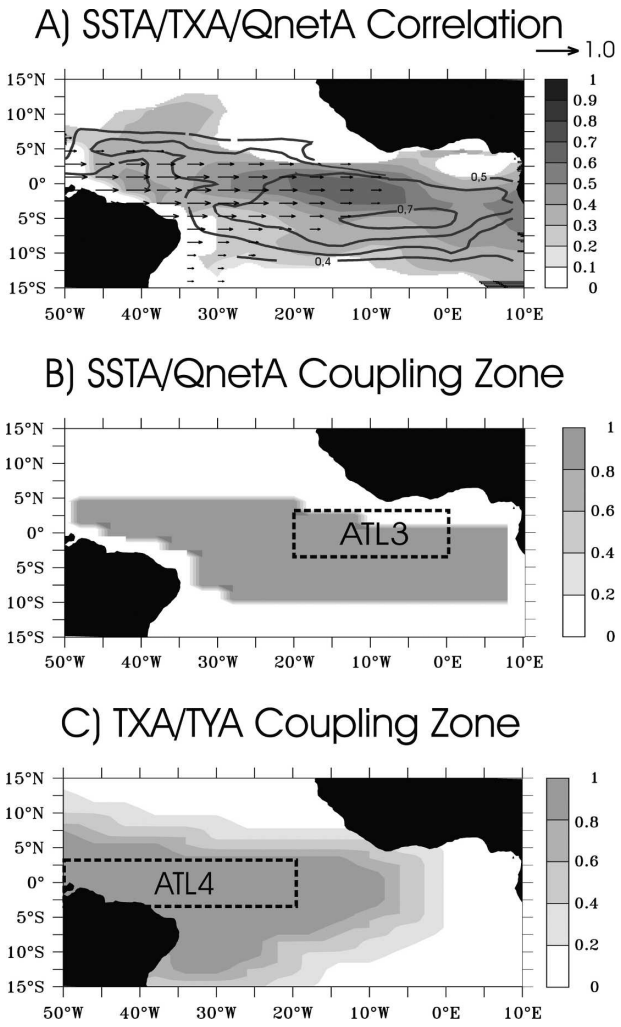

FIG. 7. (a) Significant correlation maps (at a 95% level) between QTCM-CR and ERA-40 for QnetA (shaded) and TXA (arrows, scale in the top-right corner). Overplotted is the significant correlation (at a 95% level) between OLM-CR and Reynolds SSTA, contoured every 0.1. The coupling zones for (b) SSTA and (c) QnetA and wind stress are represented in gray. For indication, the ATL3 region is drawn in a dashed line in (b) and the ATL4 region is drawn in dashed line in (c).

at the 95% level between model and observations. Note that delimited coupling zones have been used previously for theoretical ENSO studies (Mantua and Battisti 1995, among others) and forecasts (Pierce 1996). Figure 7a displays significant correlation (at a 95% level) between model simulations and observations for SSTA (contour), TXA (arrows), and QnetA (shading). It summarizes the results of Fig. 1 and Fig. 5 for the EA sector. Thus, the atmosphere passes TXA (QnetA) to OLM (MLM) over the shaded zone of Fig. 7c (Fig. 7b), while the OLM passes SSTA over the shaded zone of Fig. 7b. It is worth pointing out here that the coupling zone for QnetA and SSTA extends over the whole equatorial band so that only momentum forcing (when atmosphere passes TXA to OLM) is really impacted by the proposed coupling strategy.

Because of relatively strong ocean currents in the equatorial band, the momentum of the atmospheric forcing can be significantly increased or decreased depending on the direction of the oceanic currents. This has been taken into account following recent results showing that such an improved coupling procedure can impact CGCM simulations (Luo et al. 2005). Note also that this ensures angular momentum conservation between the atmosphere and the ocean.

For all runs presented in this paper, both model components are started from rest. To achieve a smooth transition and to reduce the shock for the air–sea adjustment, during 4 yr (1976–80) the OLM is forced by simulated wind stress anomalies, with the boundary conditions for the atmospheric component being the Reynolds SST over the globe. Then, in early 1980 (1981), OLM (QTCM) passes SSTA (QnetA) to MLM. Thus, after this 6-yr spinup, the model is fully coupled in EA. The results are analyzed starting in January 1982. Note at last that 20-member ensemble experiments were carried out for most of the model configuration presented in this study. Every time that ensemble runs were carried out, the deviation from the ensemble mean was weak over the whole period (usually less than ~2%). Therefore, for simplicity, we choose to present a single run for all the experiments presented in the following.

c. *Reference coupled run*

The model is first run in a coupled context with prescribed realistic SST outside the EA region over the 1982–2001 period. This run, referred to as TIMACS-CR, will serve as a benchmark for interpreting the results of the experiment carried out in the following. It will also tell us how the regions outside the equatorial waveguide impact the EA variability. This section also provides a preliminary analysis of the impact of air–sea interaction in EA in the presence of realistic remote forcing.

Figure 8a displays the ATL4-averaged zonal wind stress anomalies (TXA) for the TIMACS-CR experiment along with the observations (ERA-40). The coupled experiment exhibits oscillations that share many characteristics with QTCM-CR (Fig. 2) and observations. We observe a coherent timing sequence of warm and cold events. In the ATL4 region, the correlation between the simulated and the observed TXA peaks to 0.54. This corresponds to a level of significance of 99%. The rms difference does not exceed 0.86 ×

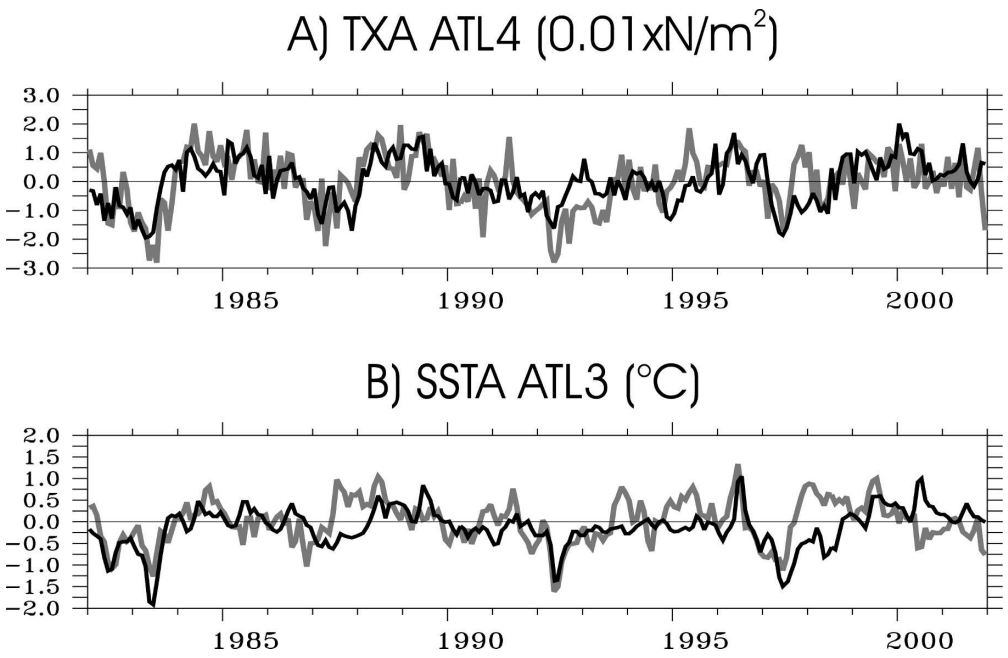

FIG. 8. (a) TIMACS-CR (black line) and ERA-40 (gray line) TXA ATL4 indices (0.01 N m^{-2}) and (b) TIMACS-CR (black line) and Reynolds (gray line) ATL3 indices (°C).

10^{-2} N m^{-2}. The comparison between simulated and observed ATL3 indices for SSTA is displayed in Fig. 8b. As for TXA, the simulated SSTA have pronounced interannual variability, with a magnitude that is comparable to the observations. The rms for ATL3 only differs by 10% for the model and the observations (rms difference of 0.50°C) and the correlation peaks to 0.41 (significant at a 98% level). However, the model does not reproduce the proper timing of the main interannual events. In particular, during the 1987 and 1997 El Niños, it misses the observed warming in 1987–88 and 1998. Note that these periods also correspond to poor simulation of zonal wind stress anomalies in ATL4. During weak El Niño activity, the model does exhibit some skills in reproducing the level of SSTA variability and some events, such as the 1992 cooling and the 1996 warming.

Considering the different response of the model in EA with regards to the period and characteristics of the remote conditions, further investigation of the local air–sea feedbacks in TIMACS in EA and remote ENSO forcing is required from specific numerical experiments. Considering the relatively large number of experiments carried out in this study, the reader is referred to Tables 1 and 2 , every time it appears necessary, for a description of the experiments and their specific use with regards to the hypothesis that is being tested. In essence, the basic structure of the experiment carried out in the following is composed of two sets of experiments. To characterize the EA ocean–atmosphere interactions simulated by TIMACS, we perform first a set of experiments that consists of switching on and off the coupling within the EA (see Table 1 and section III). Then, in order to investigate the impact of Pacific ENSO variability on the EA variability, we compare experiments with climatological SST prescribed in the tropical Pacific to experiments with interannually changing SST here (see Table 2 and section IV).

3. The Atlantic El Niño mode

This section aims to investigate the characteristics of the equatorial mode simulated by TIMACS. Several experiments (see Table 1) are carried out in order to assess whether the model SSTA variability is the result of a stable (i.e., damped) or unstable coupled mode. A forced experiment is first carried out that allows the privileged time scales of the variability in the EA to be inferred. Then, the model is run in a coupled mode in order to estimate the characteristics and stability equatorial mode simulated by TIMACS.

a. Atmospheric experiments with ATL forcing only

To document the preferred time scales and amplitude of the atmospheric response to EA SSTA over 1982–2001, a forced atmospheric simulation is first carried out. This experiment is designed such that observed SST interannual variability (1982–2001) is pre-

TABLE 1. Summary of the numerical experiments of section 3. Experiments in which the air–sea coupling is achieved in the EA are in bold. The fifth and sixth columns provide results of the comparison over the 1982–2001 period between the simulation and Reynolds SSTA and ERA-40 TXA, respectively. Unit is 0.01 N m^{-2} (°C) for TXA (SSTA) rms differences. The last column provides information on the use of the experiments in sections 2 and 3.

Expt name	Region of prescribed observed interannual forcing	Coupling efficiency in the EA	Extratropical storms (on/off)	SSTA correlation (rms difference) in ATL3	TXA correlation (rms difference) in ATL4	Used to/as
QTCM-CR	Globe	0	On	×	0.60 (0.84)	Reference run
QTCM-ATL	EA	0	On	×	0.34 (0.91)	Estimate the importance and preferred time scales of EA SST forcing
TIMACS-CR	Globe without EA	1	On	0.41 (0.51)	0.54 (0.86)	Reference run
TIMACS-CP1	None	1	On	×	×	Study the intrinsic characteristics of the equatorial mode
TIMACS-CP2	None	1	Off	×	×	Study the stability of the equatorial mode
TIMACS-CP2-Noise	Atmospheric noise originating from tropical Pacific	1	Off	×	×	Study the stability of the equatorial mode

TABLE 2. Summary of the numerical experiments of section 4. The experiments in which the air–sea coupling is achieved in the EA are in bold. The sixth and seventh columns provide the results of the comparison over the 1982–2001 period between the simulation and Reynolds SSTA and ERA-40 TXA, respectively. TXA (0.01 N m^{-2}) and SSTA (°C) rms differences. The last column provides information on the use of the experiments in section 4.

Expt name	Region of prescribed observed interannual forcing	Coupling efficiency in the EA	Coupling efficiency outside EA (slab mixed layer)	Extratropical storms (on/off)	SSTA correlation (rms difference) in ATL3	TXA correlation (rms difference) in ATL4	Used to/as
QTCM-PAC	Tropical Pacific	0	0	On	0.32 (0.59)	0.55 (0.84)	Reference run
TIMACS-PAC	Tropical Pacific	1	0	On	0.39 (0.55)	0.50 (0.88)	Study the local air–sea coupling in EA under ENSO remote forcing
QTCM-PAC-Slab	Tropical Pacific	0	1	On	-0.25 (0.57)	0.48 (0.86)	Study the impact of remote ENSO forcing over NTA
TIMACS-PAC + Slab	Tropical Pacific	1	1	On	0.40 (0.53)	0.51 (0.86)	Study the interaction between NTA and EA under ENSO remote forcing

scribed only in the EA, and elsewhere the Reynolds seasonal SST is prescribed as a boundary condition (hereafter QTCM-ATL; see Table 1). The results of this section will also aid in the interpretation of the coupled simulations performed in section 3b.

QTCM-ATL and QTCM-CR zonal wind stress anomalies (TXA), averaged in the ATL4 region, are displayed in Fig. 9a. The TXA response of the local EA forcing exhibits interannual variability 41% weaker than the QTCM-CR variability. A time–frequency analysis of QTCM-ATL and QTCM-CR TXA averaged in the ATL4 region is performed following Torrence and Compo (1998). For each frequency of the analysis, the corresponding time series is reconstructed. Then, for each time series, the correlation between QTCM-ATL and QTCM-CR, and the explained variance of the QTCM-ATL TXA ATL4 index, referenced to the QTCM-CR TXA ATL4 index variance, are calculated. The results are displayed in Figs. 9b and 9c. The zones with the largest correlation (Fig. 9b) mostly appear for comparable periods. Three frequency bands can be distinguished—an intraseasonal frequency band, periods between 12 and 36 months, and periods larger than 4.5 yr. QTCM-ATL exhibits a peak in the explained variance of the observed variability for periods between 16 and 24 months and at the semiannual period (Fig. 9c). This is consistent with Latif and Grötzner (2000), which suggest that the quasibiennial oscillation is favored in the EA. Note that a quasibiennial variability is present in the ENSO remote forcing. However, its signature is mostly prominent in the tropospheric circulation (Ropelewski et al. 1992). This is consistent with the interpretation that the quasibiennial signal simulated by QTCM-ATL for surface wind stress is most likely associated with local coupled interactions. Note also that the periods between 5 and 7 yr in QTCM-CR correlate with the 5-yr period in QTCM-ATL. This suggests a rectified effect of the ENSO variability on the EA low-frequency variability.

This result confirms that remote forcing is a source of the low-frequency variability in EA. However, enhanced variability in the 12–36-month frequency band is most likely to result from a local coupled interaction. This is further investigated in the following section from a coupled experiment that only considers explicit air–sea feedback in the EA.

b. The so-called Atlantic Niño in TIMACS

1) SPATIOTEMPORAL CHARACTERISTICS

To study the EA-coupled mode dynamics and document its preferred time scale and magnitude, a coupled run with TIMACS is performed in which we do not consider any remote interannual forcing (hereafter TIMACS-CP1; see Table 1). This means that outside EA, the Reynolds SST climatology is prescribed as boundary condition for the atmosphere, so that the EA is the only source of interannual variability.

The results for the ATL3 SST index are displayed in Fig. 10a. Interestingly, without prescribed interannual remote forcing, the model produces SSTA variability with time scales similar to that of the observations (Fig. 10b), with an albeit smaller magnitude (~50%). Figure 10d indicates that frequency bands of SSTA variability, similar to what is found for QTCM-ATL, are favored, namely, intraseasonal, 20–36 months, and 5–7 yr. TIMACS-CP1 also exhibits some energy at the annual period. It was found that the seasonal cycle produced by the model is always one order of magnitude less than the prescribed model climatology for SST, and horizontal and vertical currents. This was considered consistent with the assumptions used in MLM. The quasibiennial oscillation is also prominent (Fig. 10b). It is also worth noting the presence of energy at decadal time scales as illustrated by the 5-yr running mean of the 100-yr ATL3 SST time series (Fig. 10e).

Figure 10c presents the dominant mode of the SVD between SST and wind stress anomalies simulated by TIMACS-CP1. The spatial patterns of the mode resemble the ones derived from the observations (Fig. 3a), with a relative maximum in SSTA around (0°N, 20°W) and a meridional broadening in the Gulf of Guinea. The meridional scale of SSTA is also reasonable, although the zero line in the South Atlantic is closer to the equator than in the observations. The largest differences between the model and the observations are the SSTA maximum near the African coast and the wind stress pattern that exhibits a meridional component that is too weak. This leads to a wind patch that extends farther zonally than that observed. The southerlies in the northern (~4°N) west Atlantic are also absent in TIMACS-CP1.

The interannual variability in the eastern EA is strongest during boreal summer, when the equatorial upwelling is at a maximum and the thermocline is close to the surface (Ruiz-Barradas et al. 2000; Latif and Grötzner 2000). It is interesting to see whether the coupled model can reproduce this phase locking. Figure 11 presents a histogram plot of the warm-event occurrences in TIMACS-CP1 and the 12–36-month reconstructed time series of the observations (Torrence and Compo 1998). The threshold for a warm event is chosen to be 1.5 times the variance of the ATL3 time series (i.e., 0.23°C for TIMACS-CP1 and 0.36°C for the observations). This indicates that the model produces most warm events around June–July, whereas there is

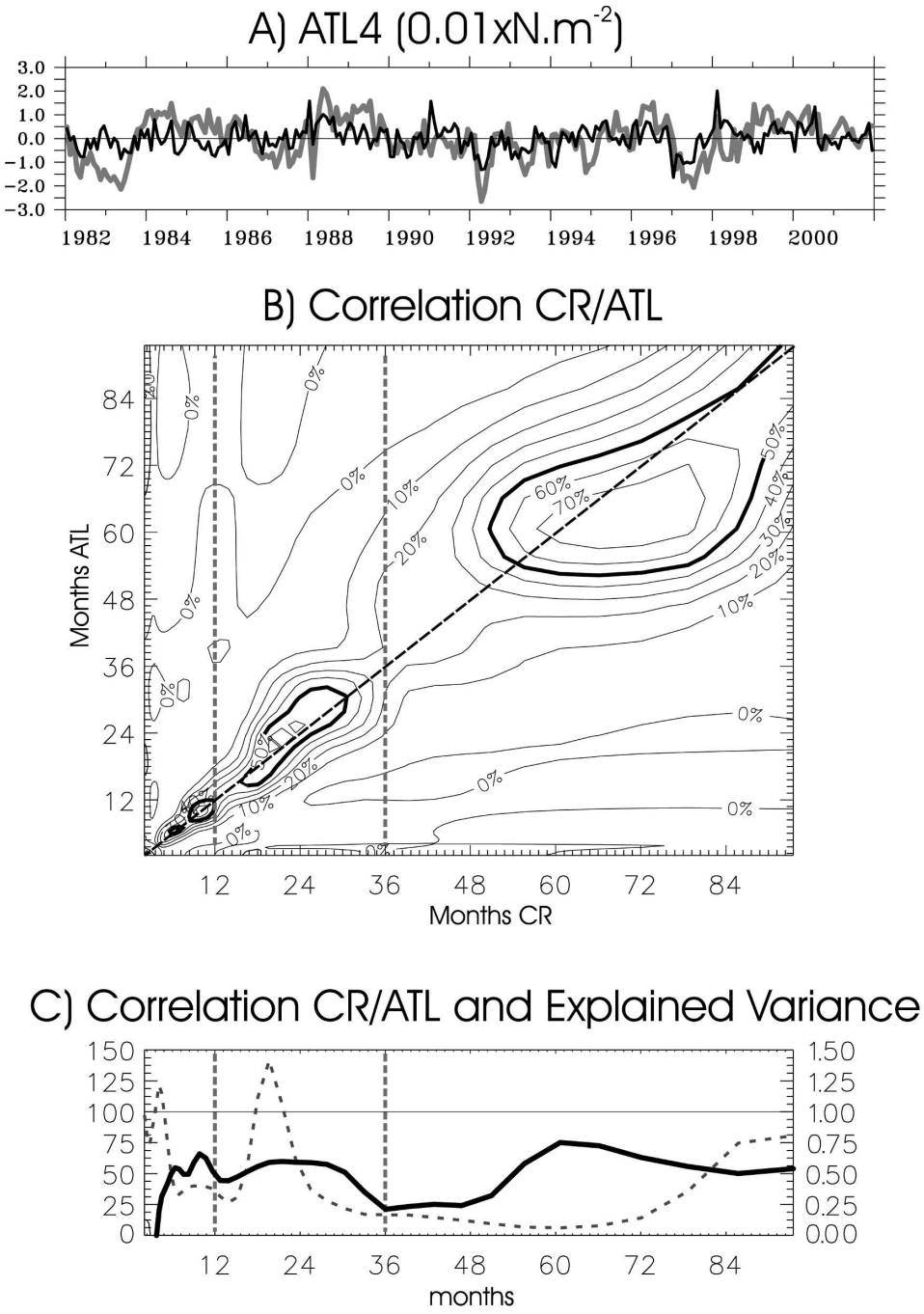

FIG. 9. (a) QTCM-ATL (black line) and QTCM-CR (gray line) ATL4 indices (0.01 N m^{-2}). (b) From the results of a wavelet analysis, for each frequency, the correlation (in %) between QTCM-ATL and QTCM-CR ATL4 indices is drawn. (c) The correlation (plain line, right scale) between QTCM-PAC and QTCM-CR ATL4 and the explained variance (dashed line, left scale) (referenced to the QTCM-CR variability) is plotted as a function of the frequency.

no significant warming in boreal spring. This is in agreement with the observations, although there is a 1-month lag between the maximum record of warm events (July for the model and August for the observations) and a broader repartition in the model than in observations in boreal summer. Note, however, that remote realistic forcing has not been included in the model, which limits the comparison between the model and observations.

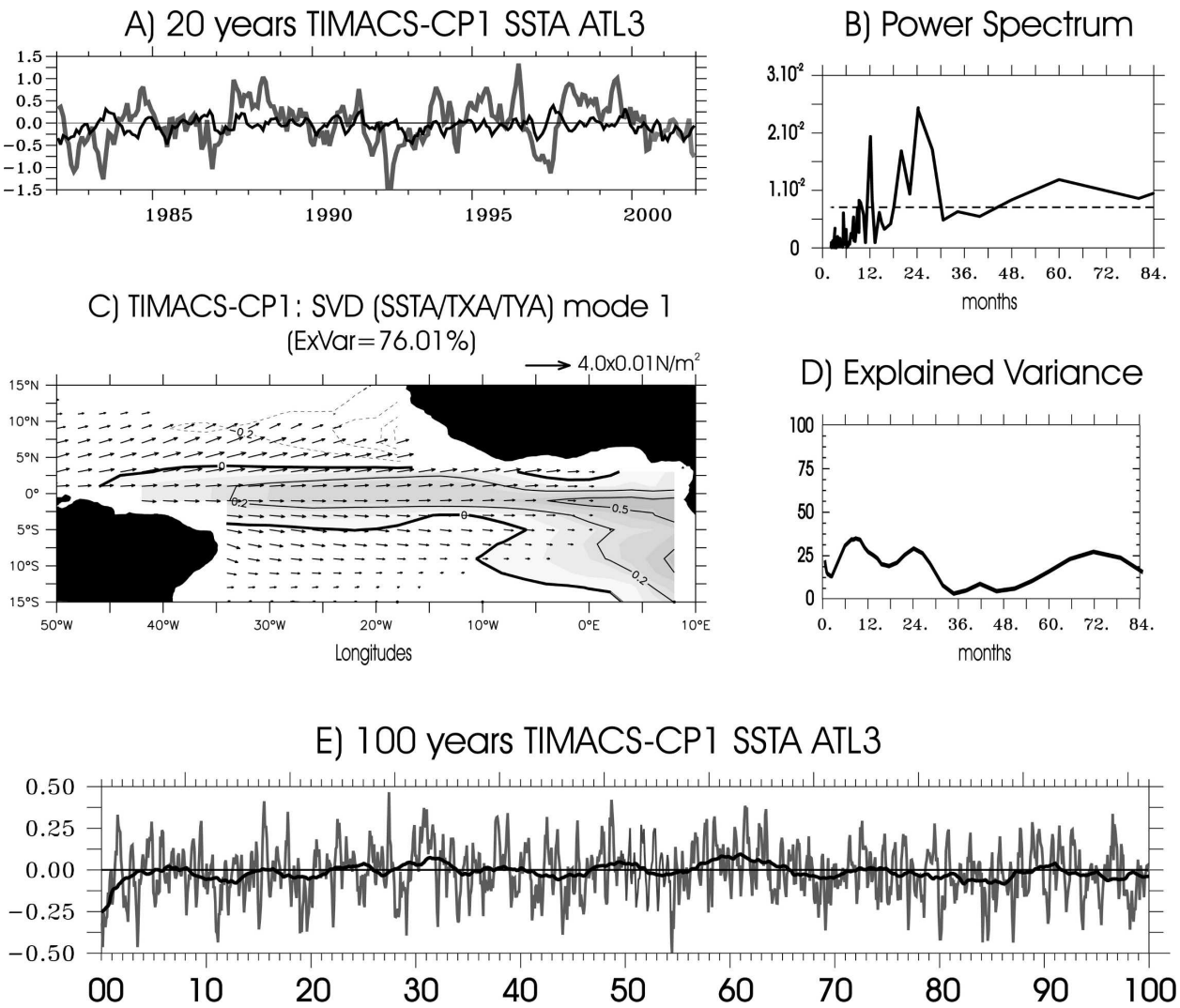

FIG. 10. (a) TIMACS-CP1 (black line) and Reynolds (gray line) SSTA ATL3 index over 1982–2001 (°C). (e) The 100-yr TIMACS-CP1 (gray line) SSTA ATL3 index, along with its 5-yr running mean (black line). (b) Its associated power spectrum (fast Fourier transform). The dashed line in the power spectra is the 95% significance level. (d) From the results of a wavelet time–frequency analysis of TIMACS-CP1 and Reynolds SSTA ATL3 indices, the explained variance, referenced to the Reynolds ATL3 variances plotted as a function of frequency. (c) The spatial structure of the dominant mode of the SVD between SSTA and wind stress anomalies of the 100-yr TIMACS-CP1 (same as in Fig. 3a).

Overall, the equatorial mode simulated by TIMACS shares many characteristics with the observations, which allows for further sensitivity tests using the model. Before addressing the issue of the remote influence of ENSO on this simulated equatorial mode, it is necessary to assess the impact of stochastic forcing on its characteristics. This is done in the following.

2) ROLE OF ATMOSPHERIC INTRASEASONAL VARIABILITY

Of particular interest in the EA sector is the part played by random noise in maintaining interannual variability. Z93 and Nobre et al. (2003) suggest that without noise, the EA mode is damped. To address this point, two model runs are carried out, in order to evaluate the stability of our coupled system and also to assess its sensitivity to stochastic forcing with regards to the experiment carried out in the previous section (see Table 1).

The first experiment consists of "damping" out the natural high-frequency variability of the atmospheric model. Lin et al. (2000) showed that the main source of intraseasonal variability in QTCM comes from the so-called evaporation–wind feedback and excitation by the

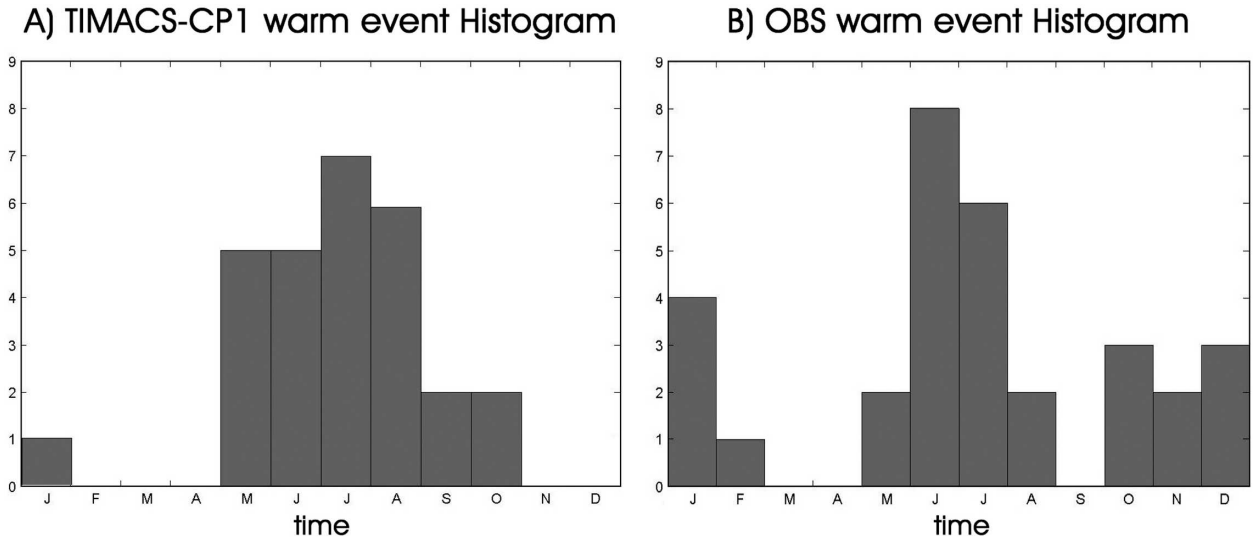

FIG. 11. Histogram plot of warm-event occurrence in ATL3 in (a) a 54-yr record of TIMACS-CP1 and (b) the high-frequency component [$f > 3(\text{yr})^{-1}$] of the Reynolds SSTA (1950–2003). The frequency decomposition/reconstruction is based on wavelet decomposition. The criterion for warm event qualification is SSTA larger than 1.5 times its variance.

extratropical storms. They proposed a methodology for turning off these two processes (see Lin et al. 2000 for details). We checked that, for the version of the model used in this paper, these two processes are still major sources of energy for the intraseasonal variability, which is a complex combination of coherent and stochastic features. Applying their method, the internal model variability in the EA is almost totally damped out. There was a ratio of $\sim 10^6$ between two climatological runs with and without extratropical disturbances for the TXA high-frequency variability in the ATL4 region. Intraseasonal anomalies were calculated from the daily model outputs, as in Lin et al. (2000). Their method is therefore applied here for turning off the evaporation–wind feedback and the extratropical disturbances. Daily averaged atmospheric model climatologies were recalculated within this new model configuration and prescribed in TIMACS to derive the fluxes anomalies that are passed to OLM [as described in section 2b(2)]. The model is forced with realistic interannual remote forcing until January 1990, and after this date climatological SST are prescribed out of EA as boundary conditions, while air–sea coupling is switched on over the EA. This model setup is called TIMACS-CP2 (see Table 1). Results are displayed in Fig. 12 for the ATL3 SST index. Until January 1990, the model presents interannual variability with and amplitude and phase that is in good agreement with TIMACS-CR variability (not shown). After this date, SSTAs weaken rapidly to reach zero within a year, indicating that atmospheric noise is required for the model to sustain oscillations. Note that increasing the coupling efficiency by up to 30% does not significantly alter this result. The SSTA still reaches zero after a few years.

To confirm this result, atmospheric noise is prescribed within the former model setup. The noise is obtained from the deviation from the daily climatology of a 10-yr-long seasonal run, so that the spatiotemporal characteristics of the intraseasonal variability are kept. This run is named TIMACS-CP2-Noise (see Table 2). Results are overplotted on Fig. 12, which shows that an oscillatory behavior is recovered after 1990, confirming the stable nature of the equatorial mode simulated in TIMACS. Several other tests, with a different noise product, were performed. In particular, following Kirtman and Schopf (1998), noise obtained from the difference between the total and the 6-month low-pass-filtered SSTAs was used as boundary forcing for the atmospheric model in the tropical Pacific sector only, allowing for transmission of high-frequency forcing over the tropical Atlantic. In such a configuration, the model also exhibits a variability after 1990, although

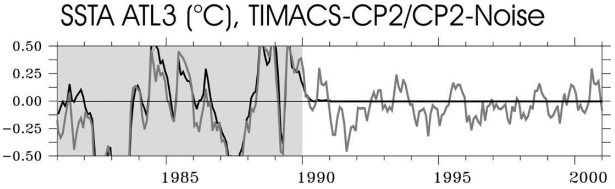

FIG. 12. TIMACS-CP2 (black line) and TIMACS-CP2-Noise (gray line) ATL3 indices (°C). Gray shading indicates the period over which the model is forced over the tropical Pacific sector.

42% weaker in magnitude than in TIMACS-CP1. The first SVD mode between the SST and wind stress anomalies in EA explains 78.5% of the covariance with a similar pattern to that of Fig. 10c (not shown). The time scales of the variability and the phase locking around July are also comparable to TIMACS-CP1, which confirms the above. These results will be further confirmed by a stability analysis presented in the discussion section (see also appendix C).

4. Pacific ENSO remote influence (1982–2001)

In light of the above results, we now investigate the impact of Pacific ENSO variability on the EA variability. In this section, only the interannual ENSO forcing over the tropical Pacific is considered. Elsewhere the Reynolds monthly seasonal SST is prescribed as a boundary condition for the atmosphere. Two regions where simulated SSTA will be superimposed on the climatological SST are the EA and the northern tropical Atlantic. A first series of experiments, in which air–sea interactions are switched off or on over the EA, is carried out and analyzed (see Table 2). The results of these experiments will serve to estimate the role of the local air–sea coupling in EA under the influence of ENSO. The role of the air–sea interaction in the NTA on the ENSO response over the tropical Atlantic is then considered through other coupled model experiments using a simple slab mixed layer for the tropical Atlantic off-equatorial regions (see Table 2). The results of these experiments will allow the role on NTA in the teleconnection pattern simulated by TIMACS to be estimated.

a. Pacific remote influence on the EA variability

To analyze the remote effect of the tropical Pacific interannual forcing without explicit local air–sea feedback in the EA, we first force QTCM with observed SST interannual variability only in the tropical Pacific (30°S–30°N). Elsewhere, the Reynolds monthly seasonal SST is prescribed as boundary conditions. This atmospheric-forced experiment is referred to as QTCM-PAC. This simulation will be further compared to the results of a twin simulation, where air–sea coupling will be turned on in EA, again with observed interannual SSTA in the tropical Pacific (hereafter TIMACS-PAC; see Table 2). This will provide an estimate of the impact of local air–sea feedbacks in EA.

The QTCM-PAC and QTCM-CR zonal wind stress anomalies (TXA) that are averaged in the ATL4 region (Fig. 13a) present similar interannual amplitude and phase, indicating that most of the low-frequency wind stress variability in the EA originates from the tropical Pacific. Correlation between ATL4 indices of QTCM-PAC and QTCM-CR is 0.69 (rms difference is 0.66×10^{-2} N m^{-2}). A time–frequency analysis similar to the one in section 3a is performed for the QTCM-CR and QTCM-PAC TXA ATL4 time series. It allows for the correlation between QTCM-CR and QTCM-PAC and the explained variance of the QTCM-PAC variability (referenced to QTCM-CR) to be computed for each frequency. Results are displayed in Fig. 13b. They confirm that QTCM-PAC reproduces the low-frequency variability of QTCM-CR (periods larger than 36 months), but it does not account for all of the higher frequencies of QTCM-CR (periods between 12 and 36 months). Thus, the 36–84-month-band reconstructed time series of the QTCM-PAC and QTCM-CR ATL4 indices are correlated at a 0.97 level (rms difference of 0.12×10^{-2} N m^{-2}). Moreover, this low-frequency component of the variability is highly correlated to ENSO ($c = -0.84$ for QTCM-PAC and $c = -0.80$ for QTCM-CR, see the Niño-3 SST index plotted in a dashed line on Fig. 13a). At a higher frequency [$f < \sim 30$ (month)$^{-1}$], there are more discrepancies between the two runs. Note, for instance, that the zonal wind anomalies in early 1998 are positive for QTCM-CR and negative for QTCM-PAC. The correlation between the QTCM-PAC and QTCM-CR ATL4 indices drops to 0.35 for the 12–36-month band (rms difference is 0.59×10^{-2} N m^{-2}).

For estimating the contribution of EA air–sea interactions, we first need to analyze the signature of the zonal wind stress variability originating from the tropical Pacific (TXA from QTCM-PAC) on the SST response in EA. QTCM-PAC monthly wind stress anomalies (hereafter PACwinds) are therefore used to force the OLM at each time step. This run is equivalent to OLM-CR [see section 2b(2)], but uses PACwinds as the wind stress forcing. The results for the ATL3 SST index are presented in Fig. 13d (black line). The ocean model simulates realistic SSTAs (see correlation in Table 2), although with less skill than when it is forced with observations (see Fig. 5b). In particular, it misses some of the brief events like the 1996 warming and the consecutive cooling and warming. This illustrates the importance of air–sea feedback processes in EA.

Next, we investigate how explicit air–sea interactions in the EA will modify the above results and consequently estimate the role of the local air–sea coupling in EA under the influence of ENSO. From the results of section 3b it is expected that local air–sea interactions in the EA increase the high-frequency component [$\sim$12–36 (month)$^{-1}$ frequency band] of the variability. It is interesting to assess whether this holds within a

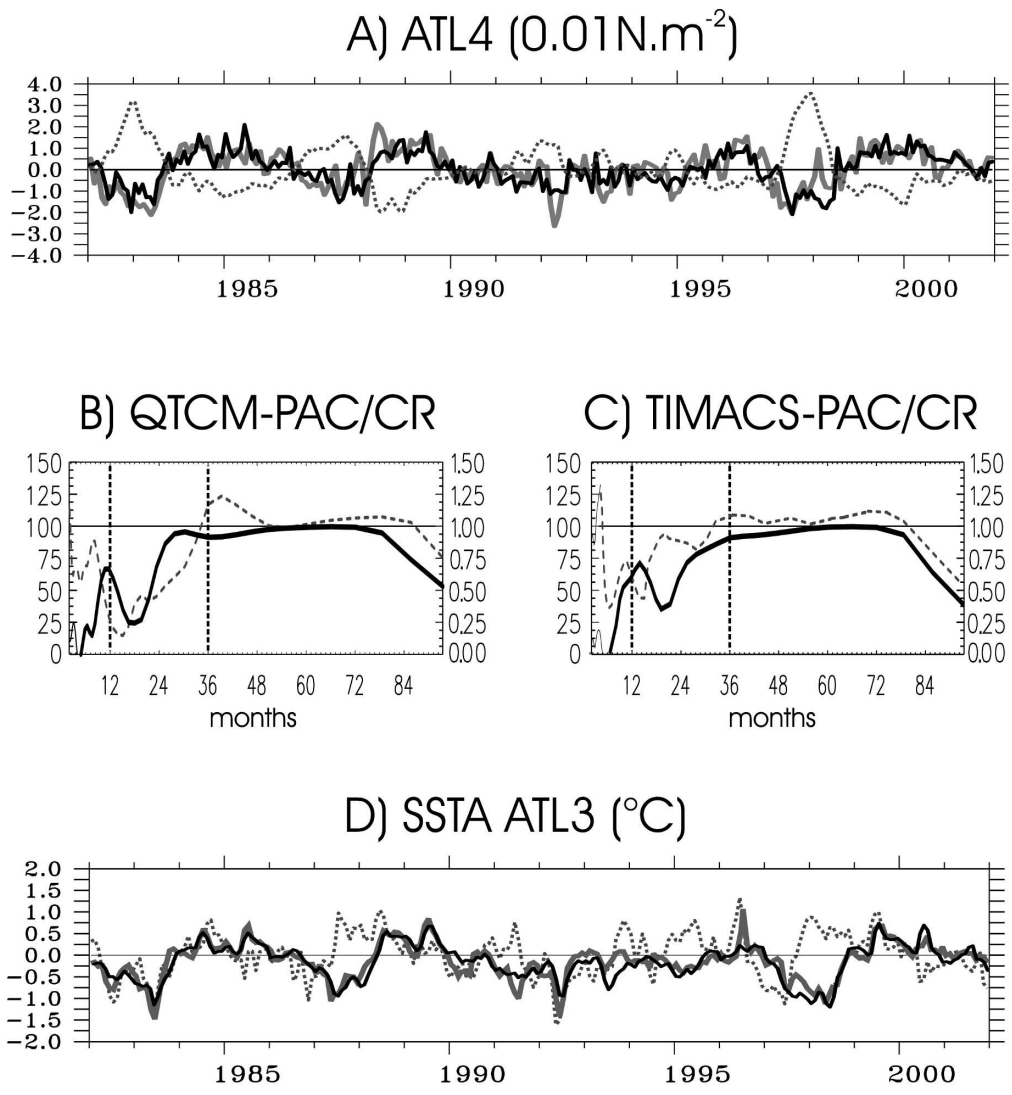

FIG. 13. (a) QTCM-PAC (black line) and QTCM-CR (gray line) TXA ATL4 indices (0.01 N m^{-2}). Reynolds Niño-3 index (°C) is plotted with a dashed gray line. The correlation (plain line) between (b) QTCM-PAC and (c) TIMACS-PAC and QTCM-CR ATL4 and the explained variance (dashed line) (referenced to the QTCM-CR variability) as a function of frequency [same as Fig. 9c]. (d) QTCM-PAC (black line), TIMACS-PAC (gray line), and Reynolds (dashed gray line) ATL3 indexes (°C).

realistic framework (i.e., under the influence of prescribed ENSO forcing) and up to what level the high-frequency variability is increased. To address these questions, we analyze the outputs of the simulation, in which the tropical Pacific interannual remote forcing is prescribed, while air–sea coupling is switched on over the EA (TIMACS-PAC). The result of TIMACS-PAC is displayed in Fig. 13d (gray line) for the SSTA ATL3 index and must be compared to results of QTCM-PAC. Taking into account air–sea interaction in EA, the total SSTA variability in TIMACS-PAC is only increased for the whole period by ~6%, as compared to QTCM-PAC. However, a closer inspection of Fig. 13d indicates that some periods in TIMAC-PAC are marked with larger variability than in QTCM-PAC. For instance, the SSTA variability is larger by 12% in 1989–96 for TIMACS-PAC as compared to QTCM-PAC. This is associated with a better simulation of some peculiar events, like the summer 1992 cooling and the June 1996 warming. Analyzing the TXA ATL4 time series from TIMACS-PAC in a similar manner reveals that the explained variance is increased by ~22% (3%) in the 12–36 (36–84) $month^{-1}$ frequency band, as expected from the effect of local air–sea interaction.

b. Role of NTA

Air–sea feedback has the potential to modify the lagged response of the tropical troposphere temperature to ENSO SST forcing. As shown in Su et al. (2005), during ENSO the pattern of tropospheric temperature warming resembles that expected from wave dynamics. On the other hand, the warming outside the tropical Pacific increases on a time scale longer than that of the atmospheric wave adjustment. It is then necessary to examine the role of the NTA where air–sea feedback through heat flux adjustment operates during El Niño events, as shown in Czaja et al. (2002) among others [see also section 2b(1)]. This region also connects the descending branch of the Atlantic Hadley circulation (Wang 2002) with the zonal atmospheric circulation in the tropical Atlantic and therefore may alter the equatorial coupled variability of TIMACS described above.

To do so, as in Su et al. (2005), a simple slab mixed layer model, where SST changes are driven by heat flux anomalies, is embedded into the system for the Atlantic regions outside the EA (i.e., for the 10°–40°N and 10°–40°S bands), following $\partial(T)_t = [Q_{\text{net}}/\rho C_p \bar{h}_{\text{mix}}(x, y, t_{12})]$, with C_p being the water heat capacity (4.18 J g^{-1} K^{-1}). In these regions, the mixed layer ocean interacts with the atmosphere via averaged SST and surface fluxes. A seasonally varying MLD $[\bar{h}_{\text{mix}}(x, y, t_{12})]$ is prescribed (de Boyer Montégut et al. 2004) to take into account the increase (decrease) of oceanic heat capacity in boreal winter (summer). Two simulations, referred as QTCM-PAC-Slab and TIMACS-PAC-Slab, are carried out with the slab mixed layer turned on and the equatorial MLM turned off and on, respectively (see Table 2). The lagged response to ENSO remote forcing in DJF is examined over the tropical Atlantic for SSTA in MAM in Fig. 14. It is compared to observations and to the results of TIMACS-PAC (i.e., without the slab mixed layer model).

The results highlight the relaxation of the northeast trade winds associated to an El Niño event in the tropical Pacific [see section 2b(1) and Fig. 4]. This leads to a warming of the SST in the NTA around March–April–May of about 0.5°C between 5° and 25°N (Fig. 14b1), associated with the reduction in evaporation (positive QnetA), which is well captured by the slab model in the NTA (Figs. 14b2 and 14b4).

Interestingly, there is no impact of air–sea feedbacks in NTA over the EA as illustrated by the similarity of the results of TIMACS-PAC and TIMACS-PAC-Slab in the equatorial band. Both model configurations tend to overestimate the cooling that follows the El Niño events. This is mostly due to the deficiency of the model in simulating the EA warming consecutive to the 1987 and 1997 El Niño events as pointed out in section 2c. On the other hand, the SSTAs in NTA for QTCM-PAC-Slab and TIMACS-PAC-Slab exhibit a different pattern, with SSTAs being shifted eastward in TIMAS-PAC-Slab as compared to QTCM-PAC-Slab. TIMACS-PAC-Slab is in better agreement with the observations because the peak of SSTAs warming and the northeast trade winds relaxation is closer to the western coast of Africa. This change in the location of the NTA warming between QTCM-PAC-Slab and TIMACS-PAC-Slab indicates a feedback between the EA variability and the meridional atmospheric circulation; the intensification of the Walker circulation in the EA results in a relaxation of the Hadley circulation (Bjerknes 1969; Wang 2002; Klein et al. 1999), leading to an eastward displacement of the zone of the northeast trade winds. This was checked by comparing the regressed maps of the meridional circulation in March–April–May over the Niño-3 index in November–December–January for the QTCM-PAC-Slab and TIMACS-PAC-Slab experiments (not shown). TIMACS-PAC-Slab is associated to both the intensification of the Walker circulation and a significant relaxation of the Hadley cell in the Northern Hemisphere, whereas this is not the case in QTCM-PAC-Slab. Consistent with this interpretation, the timing of the maximum SSTA response in the NTA (white dashed square in Fig. 14b1) reveals that SSTAs peaks ~2 months later in TIMACS-PAC-Slab than in QTCM-Slab. Here, again, this better fits the observations. This suggests that the ENSO response over the NTA is delayed by air–sea coupled processes in the EA, as compared to the time it takes the atmospheric ENSO response to reach the NTA through wave dynamics (i.e., a couple weeks). It also illustrates the complex interaction between NTA, EA, and the background remote forcing of ENSO.

5. Discussion and conclusions

The tropical Atlantic low-frequency variability was studied using an intermediate ocean–atmosphere coupled system that models the following three fundamental processes: 1) the transmission of the remote ENSO influence over the tropical Atlantic, 2) the coupled instabilities associated with wave dynamics and heat fluxes in the equatorial band, and 3) the air–sea feedback associated with heat flux only in the northern tropical Atlantic. Each component of the system was carefully validated from observations and other model outputs (ID04), allowing for a quantitative estimate of the impacts of the ENSO remote forcing on the tropical Atlantic variability and of the air–sea interactions within the EA. First, our results confirm earlier results

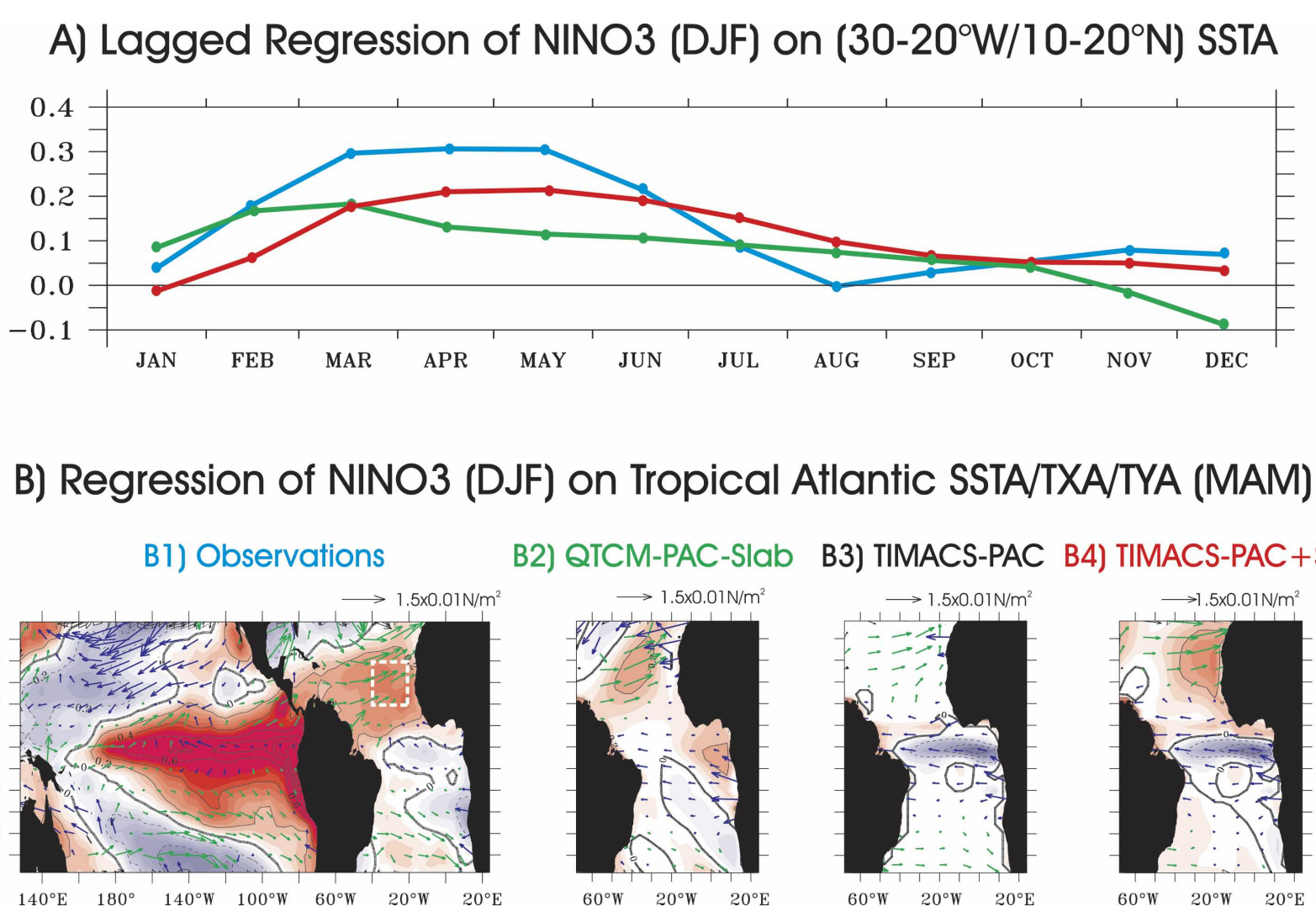

FIG. 14. (a) Lagged linear regression of normalized observed Niño-3 (DJF) index onto SSTA in the (10°–20°N, 30°–20°W) region for the observations (blue), QTCM-Slab (green), and TIMACS-Slab (red). Unit: °C. (b) Lagged linear regression of normalized observed Niño-3 (DJF) index onto SSTA and wind stress anomalies in MAM for the (b1) observations, (b2) QTCM-PAC-Slab, (b3) TIMACS-PAC, and (b4) TIMACS-PAC-Slab. SSTAs are shaded every 0.05°C and contoured every 0.2°C. The wind stress anomalies are represented with arrows (scale in the top-right corner, units are 0.01 N m^{-2}).

obtained within different modeling frameworks. In particular, the equatorial mode (or Atlantic El Niño) is stable and requires ENSO remote forcing and/or atmospheric noise to be excited (Z93; Nobre et al. 2003). Our study suggests that ENSO is the dominant source of the EA variability in the 36–84 month^{-1} frequency band. Over the whole 1982–2001 period and for the whole frequency spectrum of the variability, it was estimated that the local air–sea interaction contributes to ~6% of the SSTA variability in EA. It peaks to ~12% for the 1989–96 period of "weaker" El Niño activity.

The equatorial mode in the model has been documented with a focus on the preferred time scales to which it is associated. It is shown that the periods from 12 to 36 months are favored for zonal wind stress and SST variability, which is partly due to the summer phase locking induced by the interaction between the interannual variability and the seasonal cycle. Such a damped oscillation at quasibiennial time scales is consistent with the results of a "two stripped down" simple model (Jin 1997a,b) configured to the EA (see appendix C for details). This theoretical consistency check for explaining the privileged time scales of the variability in the EA of course presents limitations owed in part to the complex geometry of the Atlantic basin, which is not symmetrical about the equator. The relative importance of heat flux forcing as compared to the advection terms for controlling SST changes is also not considered within the conceptual model. However, it suggests that the frequency, growth rate, and spatial pattern (i.e., the nature of the air–sea interaction) of the leading coupled mode in the EA is controlled by the strength of the two coupled feedbacks mentioned above. This is similar to the tropical Pacific (An and Jin 2001). This may enlarge the scope of the approaches for investigating the EA variability. In particular, with respect to its low-frequency modulation, a similar methodology to An and Jin (2000) could be tested to investigate the interdecadal variability associated to the equatorial wave dynamics in the Atlantic.

The study also addresses the problem of the connections between the EA variability and the NTA warming, generally observed in boreal spring consecutive with an El Niño event. Model results suggest that, whereas the EA variability is not sensitive to NTA variability, the characteristics of the NTA warming in boreal spring depends on the response to ENSO forcing in the EA. In the model, the effect of air–sea coupling in the EA is to extend the NTA warming farther to the east and to delay it by a couple of months, consistently with observations and a recent modeling study (Su et al. 2005). Although not shown, experiments with idealized periodic ENSO remote forcing (typical of the strong

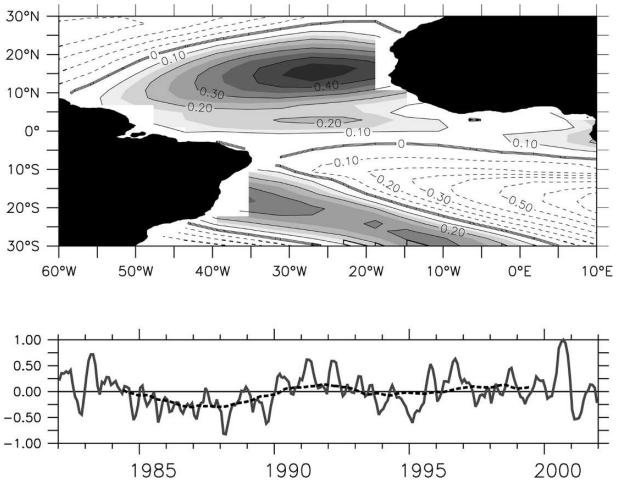

FIG. 15. Third EOF mode of TIMACS-PAC-Slab SSTA (1982–2001). (top) The spatial structures of SSTAs are contoured every 0.1°C and positive SSTAs are shaded every 0.05°C. (bottom) The associated normalized time series are represented, along with its 5-yr running mean (dashed line). The percentage of covariance explained by the mode is indicated on top of the plot.

1997 El Niño or the weak and central 1992 El Niño) also exhibit such characteristics. This indicates that the NTA variability is, to some extent, controlled by the EA interannual variability. This may have consequences for the interpretation of the so-called dipole mode in the tropical Atlantic. In fact, an EOF analysis of SSTA from TIMAC-PAC-Slab reveals a dipolelike structure for the third mode (Fig. 15). The first two modes better capture the equatorially confined variability (not shown). Interestingly, the associated time series of the third mode exhibits a prominent interdecadal oscillation. Note that similar characteristics are found for the experiments with idealized periodic ENSO remote forcing mentioned above (not shown). Despite model flaws [in particular, a tendency to produce too-cold events after El Niños (cf. Fig. 14)], these results suggest that part of the interhemispheric mode of variability may be explained by coupled processes within the tropical Atlantic, and that the ENSO remote forcing behaves as a triggering process of the interaction between the EA and the NTA. How external sources of the interdecadal variability [North Atlantic Oscillation (NAO), Pacific decadal oscillation (PDO), and others] superimpose on this mechanism needs to be further investigated. Considering the magnitude of the interdecadal variability in the model and observations, further improvement of the model physics may be necessary. For instance, the model overestimates the ENSO response in the EA, which may be partly due to the fact that topographic effects over the Andes are not resolved in the baroclinic equations (see Zeng et al.

2000 for details) and that the meridional wind stress variability is underestimated. Along with the investigation of the extratropical forcing, such improvement of the model may help to understand why the model fails to simulate realistic SSTA in the EA after the 1987 and 1997 El Niño events.

Despite these limitations, however, it is striking that, considering the relatively simple physics of TIMACS, the model simulates the dominant aspects of the tropical Atlantic variability and related ENSO teleconnections. This, in particular, is encouraging for further study of interbasin influences at decadal-to-interdecadal time scales that requires long-term simulations.

Acknowledgments. This study is part of the Ph.D. thesis of Dr. S. Illig. The authors are particularly indebted to fruitful discussions with Dr. S. E. Zebiak at the early stage of this study and to the thoughtful review of the manuscript by Dr. D. Neelin. The authors are also grateful to Nadia Ayoub and Frederic Marin, for their high-quality advice and fruitful discussions. Dr. S. I. An is acknowledged for his help designing the two-stripped-down model for the equatorial Atlantic. The authors thank the whole CLIPPER project team for the model outputs that were so kindly provided. They also thank CERSAT and AVISO for the altimetric data. ERA-40 data used in this study have been provided by ECMWF. They would also like to acknowledge Yves du Penhoat and Francis Auclair for their help. Dr. H. Su and Dr. Katrina Hales are thanked for their constructive advice during the course of this study and their help validating the high-resolution version of QTCMV1.2. The authors also thank J. D. Neelin, Hui Su, and J. E. Meyerson for sharing their prepublished manuscript. Discussions with D. Y. Gushchina were also greatly appreciated. Josh Willis is acknowledged for his careful reading of the manuscript.

APPENDIX A

Validation of the Anomalous Subsurface Temperature Formulation

Simulated subsurface temperature anomalies (T_{sub}) are derived from the baroclinic mode contributions to sea level anomalies (sl_n), assuming that thermocline anomalies are equivalent to the isotherm vertical displacement and using the hydrostatic equations (cf. Dewitte 2000),

$$T_{\text{sub}} = \alpha_T^{-1} \sum_{n=1}^{6} \text{sl}_n \times \partial_z \{F_n[\max(\overline{h}_{\text{mix}}, 50\text{ m})]\}$$

[see section 2b(2) for notations].

The following illustrates the skill of such a formulation. Because the proposed formulation depends on the baroclinic mode contributions to pressure anomalies that cannot be derived directly from observations, a vertical mode decomposition of the CLIPPER dataset has been used for the validation (see ID04 for details). The resulting anomalous vertical gradient T_z is then calculated as $T_z^{\text{obs}} = (T^{\text{obs}} - T_{50\text{ m}}^{\text{obs}}/50\text{ m})$ and compared to the observed anomalous vertical gradient derived from the TAOSTA dataset. Statistics are provided in Fig. A1 along the equator for the 1981–98 period. As a benchmark, we present the results of the parameterization of Z93, in which the thermocline depth is derived from CLIPPER. Figure A1 indicates that the proposed formulation is successful in simulating realistic subsurface temperature along the equator, with better skill than with the Z93 parameterization in the central EA. For instance, correlation (rms difference) increased (decreased) by 0.4 (0.2°C) at 25°W compared to the results of the Z93 parameterization.

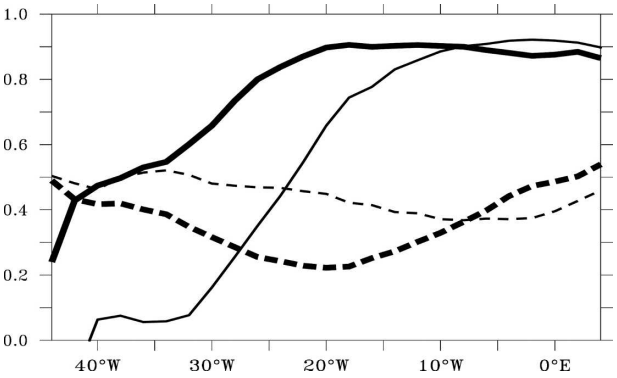

FIG. A1. Comparison between CLIPPER subsurface temperature (50 m) and the results of model parameterizations along the equator. Correlation between CLIPPER and the "new" (Z93) parameterization is displayed in plain thick (thin) line, while the rms difference (°C) is displayed in dashed thick (thin) line.

APPENDIX B

Oceanic Model Climatologies

The seasonal surface currents $\overline{u}$, $\overline{v}$ and $\overline{w}$ prescribed in the MLM were obtained by forcing the OLM with monthly mean climatological winds from ERA-40. The seasonal zonal currents are compared to the currents derived from satellite data of the Ocean Surface Current Analyses-Real Time (OSCAR; information available online at http://www.oscar.noaa.gov; see ID04 for the data description). An estimation of seasonal vertical currents is derived from CLIPPER and is used for the comparison with OLM. Results are presented as Hovmoeller plots along the equator in Fig. B1. The seasonal variability simulated by OLM generally compares well with the estimates from observations and

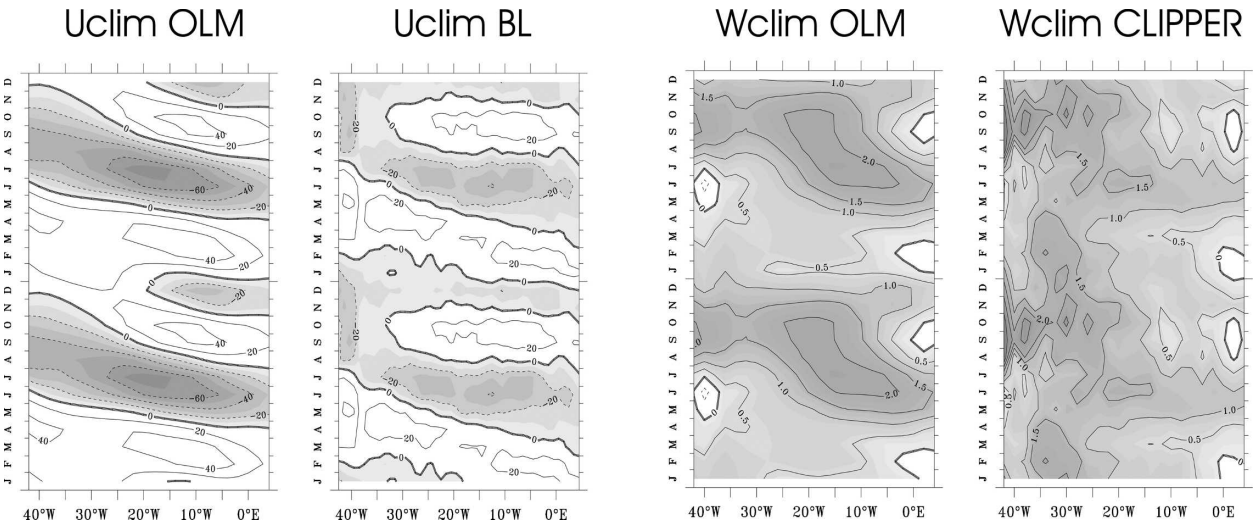

FIG. B1. Longitude time plot of currents climatologies along the equator. For clarity, the climatologies are repeated. Prescribed surface zonal current climatology from the OLM, along with the satellite-derived surface zonal current climatology (F. Bonjean 2004, personal communication) is displayed on the two left panels. Negative values are shaded. Unit: cm s^{-1}. On the right two panels, prescribed vertical current climatology from the OLM, along with the CLIPPER vertical current climatology is displayed. CLIPPER vertical currents are computed at 50-m depth. Unit: m day^{-1}.

OGCM outputs in terms of phase relationship. For instance, strong westward surface currents appear around June–July in association with the intensification of the trade winds, while upwelling is maximum at the same period. Westward-propagating features are prominent in all fields and compare well with the model; the correlation coefficient averaged along the equator reaches 0.76 (0.69) for the zonal current (vertical velocity). The largest discrepancy is found for the magnitude of the variability, which is larger for OLM than for the estimates from observation and CLIPPER. Whether or not this is a model flaw needs to be further investigated. In the absence of better datasets with which to compare, and because they lead to a realistic simulation of SSTA (see Fig. 5), these climatologies are used in the model.

APPENDIX C

An Equatorial Ocean Recharge Paradigm for the Equatorial Atlantic

At the first order, the large-scale coupled oscillating modes of the tropical oceans are controlled by two major processes known as the thermocline feedback and the zonal advective feedback (An and Jin 2001). The thermocline feedback leads to a coupled mode through the merging of the damped SST mode and ocean adjustment mode, while the zonal advective feedback tends to destabilize the gravest ocean basin mode. The characteristics of the leading coupled mode (frequency, growth rate, and spatial pattern) are controlled by the relative strength of these two coupled feedbacks. Jin and An (1999), An and Jin (2000) and An and Jin (2001) have largely interpreted the equatorial Pacific variability in light of this diagnostic. Here, we take advantage of this formalism and apply it to the EA in order to infer theoretical material for the interpretation of the equatorial mode.

The Jin (1997b) stripped-down conceptual model is thus adapted to the EA basin. We derive the model parameter value from TIMACS and observations in the EA. We will review the main characteristics of the stripped-down model of Jin (1997b). For a more detailed description and the notations the reader is referred to Jin (1997a,b).

As shown in Jin (1997a,b), the ocean dynamics equation for the thermocline depth anomalies along the equator (h_e) and in the off-equator strip, centered at $y_n = 2$ (h_n), can be written as

$$\begin{cases} (\partial_t + \varepsilon_m)(h_e - h_n) + \partial_x he = \tau_{\mathrm{xe}} \\ (\partial_t + \varepsilon_m)h_n + \partial_x h_n/{y_n}^2 = \partial_y(\tau_x/y)|_{y=y_n} \end{cases}, \quad \text{with wave reflection conditions,} \quad \begin{cases} h_e = r_W h_n \\ h_n = r_E h_e \end{cases}.$$

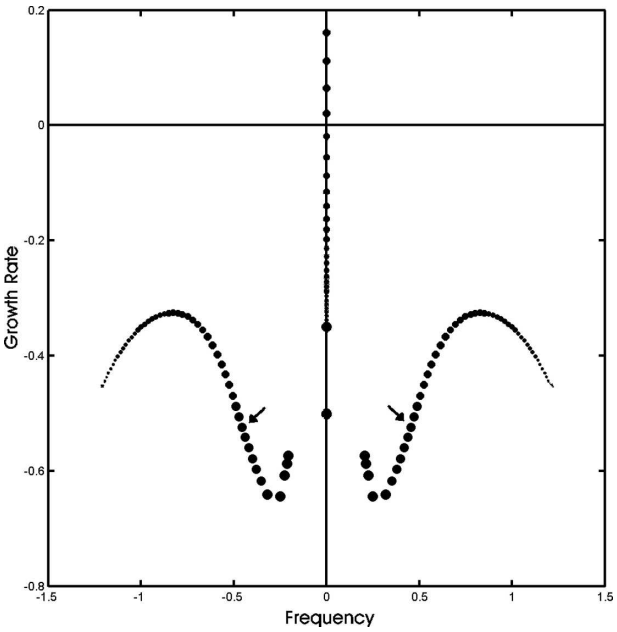

FIG. C1. Collective plot of eigenvalues for the leading eigenmodes. Ocean–atmosphere coupling efficiency is represented by mark size (smallest mark is for weakly coupled experiments, increment is 0.025, coupling efficiency of 1.0 is highlighted with arrows). Axes are frequency and growth rate (yr^{-1}). Dividing the frequency by $\pi/3$ yields the period in years. The parameters are $r_W = 0.6$ and $r_E = 0.8$.

Here $\tau_{xe}(x)$ is the zonal wind stress anomaly evaluated along the equatorial strip. With the second baroclinic mode being the most energetic in the EA (ID04), the phase speed of the second baroclinic mode ($c = 1.34$) was chosen for the oceanic Rossby deformation radius and the damping rate ($\varepsilon_m = 1/10.45$ month^{-1}).

An and Jin (2001) coupled the former conceptual ocean model to a simplified mixed layer and atmospheric model. The changes of SST along the equator (T_e) are described by a linearized equation about an upwelling climate state [$\overline{w_1}(x)$] and the zonal gradient of mean SST [$\partial\overline{T}(x)$] in a constant-depth mixed layer ($H_{1.5} = 50$ m), $\partial_t T_e = -c(x)T_e + \gamma(x)h_e + a(x)(h_e - h_n)$, with $a(x) = -\partial\overline{T}(x)/H_{1.5}$, $\gamma(x) = \gamma_0(x)\overline{w_1}/H_{1.5}$, and $c(x) = \varepsilon_T + \overline{w}_1/H_{1.5}$ ($\varepsilon_T = 1/125$ days^{-1}).

All of the parameters required for this conceptual model (see An and Jin 2001 for details) were derived from the TIMACS prescribed climatologies (see appendix B) and parameterizations (see appendix A). As in An and Jin (2000), an empirical atmospheric model of the equatorial strip describing the linear relationship between SST and wind stress anomalies based on the ERA-40 data in the 1°S–1°N equatorial band is used.

The linear eigensolutions of the two-strip model are calculated numerically with a 2° resolution in longitude and using a first-order upstream scheme. Results as displayed in Fig. C1 for a particular set of parameters. Although the results are sensitive to the values of the reflection efficiency at the meridional boundaries, the solution of the system in reasonable parameter ranges leads to negative growth rate (i.e., stable) modes. At weak coupling efficiency (i.e., no air–sea interaction), one can observe the signature of the damped basin mode. For realistic coupling efficiency (i.e., ~1.0), the solution of the system highlights a stable mode oscillating at frequencies in the 20–30 month^{-1} range.

REFERENCES

AchutaRao, K., C. Covey, C. Doutriaux, M. Fiorino, P. Gleckler, T. Phillips, K. Sperber, and K. Taylor, 2004: An appraisal of coupled climate model simulations. Lawrence Livermore National Laboratory Tech. Rep. UCRL-TR-202550, 197 pp.

An, S.-I., and F.-F. Jin, 2000: An eigen analysis of the interdecadal changes in the structure and frequency of ENSO mode. *Geophys. Res. Lett.,* **27,** 2573–2576.

——, and ——, 2001: Collective role of thermocline and zonal advective feedbacks in the ENSO mode. *J. Climate,* **14,** 3421–3432.

Barnier, B., and the CLIPPER Project Team, 2000: 1/6° reference experiment, 1/6 Atlantic circulation model forced by the ECMWF climatology: Preliminary results. LEGI Rep. CLIPPER-R2-2000. [Available online at http://www.ifremer.fr/lpo/clipper/result16/atl6/projet_clipper.htm.]

Bjerknes, J., 1969: Atmospheric teleconnections from the tropical Pacific. *Mon. Wea. Rev.,* **97,** 163–172.

Bretherton, F. P., R. E. Davis, and C. B. Fandry, 1976: A technique for objective analysis and design oceanographic experiments applied to mode-73. *Deep-Sea Res.,* **23,** 559–582.

Cane, M. A., and R. J. Patton, 1984: A numerical model for low frequency equatorial dynamics. *J. Phys. Oceanogr.,* **14,** 1853–1863.

Cassou, C., and L. Terray, 2001: Dual influence of Atlantic and Pacific SST anomalies on the North Atlantic/Europe winter climate. *Geophys. Res. Lett.,* **28,** 3195–3198.

Chang, P., L. Ji, and H. Li, 1997: A decadal climate variation in the tropical Atlantic Ocean from thermodynamics air-sea interactions. *Nature,* **385,** 516–518.

——, R. Saravanan, and L. Ji, 2003: Tropical Atlantic seasonal predictability: The role of El Niño remote influence and thermodynamic air-sea feedback. *Geophys. Res. Lett.,* **30,** 1501, doi:10.1029/2002GL016119.

Czaja, A., P. Van der Vaart, and J. Marshall, 2002: A diagnostic study of the role of remote forcing in tropical Atlantic variability. *J. Climate,* **15,** 3280–3290.

de Boyer Montégut, C., G. Madec, A. S. Fischer, A. Lazar, and D. Iudicone, 2004: Mixed layer depth over the global ocean: An examination of profile data and a profile-based climatology. *J. Geophys. Res.,* **109,** C12003, doi:10.1029/2004JC002378.

Delecluse, P., J. Servain, C. Levy, K. Arpe, and L. Bengtsson, 1994: On the connection between the 1984 Atlantic warm event and the 1982-83 ENSO. *Tellus,* **46A,** 448–464.

Dewitte, B., 2000: Sensitivity of an intermediate ocean-atmosphere coupled model of the tropical pacific to its oceanic vertical structure. *J. Climate,* **13,** 1562–1581.

Drévillon, M., C. Cassou, and L. Terray, 2003: Model study of the

wintertime atmospheric response to fall tropical Atlantic sea-surface-temperature anomalies. *Quart. J. Roy. Meteor. Soc.,* **129,** 2591–2611.

Enfield, D. B., and D. A. Mayer, 1997: Tropical Atlantic sea surface temperature variability and its relation to El Niño-Southern oscillation. *J. Geophys. Res.,* **102,** 929–945.

Fontaine, B., and S. Janicot, 1999: Observed and modeled surface variability in the tropical Atlantic region and its rainfall impacts. *Climate Dyn.,* **15,** 451–473.

Gill, A. E., 1982: *Atmosphere–Ocean Dynamics*. Academic Press, 662 pp.

Gushchina, D. Yu., and B. Dewitte, 2005: Interannual climate variability and teleconnections in the quasi-equilibrim tropical circulation model. *Izv. Atmos. Oceanic Phys.,* **41,** 435–463.

Hisard, P., 1980: Observation de réponses de type "El Niño" dans l'Atlantique tropical oriental-Golfe de Guinée. *Ocean Acta,* **3,** 69–78.

Houghton, R. W., and Y. Tourre, 1992: Characteristics of low-frequency sea surface temperature fluctuations in the tropical Atlantic. *J. Climate,* **5,** 765–771.

Huang, B., 2004: Remotely forced variability in the tropical Atlantic Ocean. *Climate Dyn.,* **23,** 133–152.

Illig, S., B. Dewitte, N. Ayoub, Y. du Penhoat, G. Reverdin, P. De Mey, F. Bonjean, and G. S. E. Lagerloef, 2004: Inter-annual Long Equatorial Waves in the Tropical Atlantic from a High Resolution OGCM Experiment in 1981-2000. *J. Geophys. Res.,* **109,** C02022, doi:10.1029/2003JC001771.

Janicot, S., A. Harzallah, B. Fontaine, and V. Moron, 1998: Forcing of equatorial Atlantic and Pacific surface temperatures on West-African monsoon dynamics in July-August (1958-1989). *J. Climate,* **11,** 1874–1882.

Jin, F.-F., 1997a: An equatorial ocean recharge paradigm for ENSO. Part I: Conceptual model. *J. Atmos. Sci.,* **54,** 811–829.

——, 1997b: An equatorial ocean recharge paradigm for ENSO. Part II: A stripped-down coupled model. *J. Atmos. Sci.,* **54,** 830–846.

——, and S.-I. An, 1999: Thermocline and zonal advective feedback within the equatorial ocean recharge oscillator model for ENSO. *Geophys. Res. Lett.,* **26,** 2989–2992.

Kirtman, B. P., and P. S. Schopf, 1998: Decadal variability in ENSO predictability an prediction. *J. Climate,* **11,** 2804–2822.

Klein, S. A., B. J. Soden, and N.-C. Lau, 1999: Remote sea surface temperature variations during ENSO: Evidence for tropical atmospheric bridge. *J. Climate,* **12,** 917–932.

Latif, M., and T. P. Barnett, 1995: Interactions of the tropical Oceans. *J. Climate,* **8,** 952–964.

——, and A. Grötzner, 2000: The equatorial Atlantic oscillation and its response to ENSO. *Climate Dyn.,* **16,** 213–218.

Levitus, S., and Coauthors, 1998: *Introduction*. Vol. 1, *World Ocean Database 1998,* NOAA Atlas NESDIS 18, 346 pp.

Lin, J. W.-B., J. D. Neelin, and N. Zeng, 2000: Maintenance of tropical intraseasonal variability: Impact of evaporation-wind feedback and mid-latitude storms. *J. Atmos. Sci.,* **57,** 2793–2823.

Luo, J.-J., S. Masson, E. Roeckner, G. Madec, and T. Yamagata, 2005: Reducing climatology bias in a ocean–atmosphere CGCM with improved coupling physics. *J. Climate,* **18,** 2344–2360.

Mantua, N. J., and D. S. Battisti, 1995: Aperiodic variability in the Cane-Zebiak coupled ocean-atmosphere model: Ocean-atmosphere interactions in the western Pacific. *J. Climate,* **8,** 2897–2927.

Merle J. M., M. Fieux, and P. Hisard, 1980: Annual signal and inter-annual anomalies of sea surface temperatures in the eastern equatorial Atlantic ocean. *Deep-Sea Res.,* **26** (GATE Suppl.), 77–102.

Neelin, J. D., and N. Zeng, 2000: A quasi-equilibrium tropical circulation model-formulation. *J. Atmos. Sci.,* **57,** 1741–1766.

——, and H. Su, 2005: Moist teleconnection mechanisms for the tropical South American and Atlantic sector. *J. Climate,* **18,** 3926–3950.

——, C. Chou, and H. Su, 2003: Tropical drought regions in global warming and El Niño teleconnections. *Geophys. Res. Lett.,* **30,** 2275, doi:10.1029/2003GLO018625.

Nobre, P., and J. Shukla, 1996: Variations of sea surface temperature, wind stress, and rainfall over the tropical Atlantic and South America. *J. Climate,* **9,** 2464–2479.

——, S. E. Zebiak, and B. P. Kirtman, 2003: Local and remote sources of Tropical Atlantic variability as inferred from the results of a hybrid ocean-atmosphere coupled model. *Geophys. Res. Lett.,* **30,** 8008, doi:10.1029/2002GL015785.

Philander, S. G. H., 1986: Unusual conditions in the tropical Atlantic Ocean in 1984. *Nature,* **322,** 236–238.

Pierce, D. W., 1996: The Hybrid Coupled Model, version 3: Technical notes. Scripps Institution of Oceanography Reference Series 96-27, 66 pp.

Reynolds, R. W., and T. M. Smith, 1994: Improved global sea surface temperature analyses using optimum interpolation. *J. Climate,* **7,** 929–948.

Ropelewski, C. F., M. S. Halpert, and X. Wang, 1992: Observed tropospheric biennial variability in the global Tropics. *J. Climate,* **5,** 594–614.

Ruiz-Barradas, A., J. A. Carton, and S. Nigam, 2000: Structure of inter-annual-to-decadal climate variability in the tropical Atlantic sector. *J. Climate,* **13,** 3285–3297.

Saravanan, R., and P. Chang, 2000: Interaction between tropical Atlantic variability and El Niño–Southern Oscillation. *J. Climate,* **13,** 2177–2194.

Sciremammano, F., Jr., 1979: A suggestion for the presentation of correlations and their significance. *J. Phys. Oceanogr.,* **9,** 1273–1276.

Servain, J., 1991: Simple climatic indices for the tropical Atlantic Ocean and some applications. *J. Geophys. Res.,* **96,** 15 137–15 146.

——, I. Wainer, J. P. McCreary, and A. Dessier, 1999: Relationship between the equatorial and meridional modes of climatic variability in the tropical Atlantic. *Geophys. Res. Lett.,* **26,** 485–488.

——, ——, H. L. Ayina, and H. Roquet, 2000: The relationship between the simulated climatic variability modes of the tropical Atlantic. *Int. J. Climatol.,* **20,** 939–953.

Smith, T. M., R. W. Reynolds, R. E. Livezey, and D. C. Stokes, 1996: Reconstruction of historical sea surface temperatures using empirical orthogonal functions. *J. Climate,* **9,** 1403–1420.

Su, H., and J. D. Neelin, 2002: Teleconnection mechanisms for tropical Pacific descent anomalies during El Niño. *J. Atmos. Sci.,* **59,** 2682–2700.

——, ——, and C. Chou, 2001: Tropical teleconnection and local response to SST anomalies during the 1997-1998 El Niño. *J. Geophys. Res.,* **106** (D17), 20 025–20 043.

——, ——, and J. E. Meyerson, 2005: Mechanisms for lagged atmospheric response to ENSO SST forcing. *J. Climate,* **18,** 4195–4215.

Sutton, R. T., S. P. Jewson, and D. P. Rowell, 2000: The elements

of climate variability in the tropical Atlantic region. *J. Climate,* **13,** 3261–3284.

Torrence, C., and G. P. Compo, 1998: A practical guide to wavelet analysis. *Bull. Amer. Meteor. Soc.,* **79,** 61–78.

Vauclair, F., and Y. du Penhoat, 2001: Inter-annual variability of the upper layer of the Atlantic Ocean from *in situ* data between 1979 and 1999. *Climate Dyn.,* **17,** 527–546.

Wang, C., 2002: Atmospheric circulation cells associated with El Niño–Southern Oscillation. *J. Climate,* **15,** 399–419.

Weare, B. C., 1977: Empirical orthogonal analysis of Atlantic Ocean surface temperatures. *Quart. J. Roy. Meteor. Soc.,* **103,** 467–478.

Xie, S.-P., and J. A. Carton, 2004: Tropical Atlantic variability: Patterns, mechanisms, and impacts. *Ocean–Atmosphere Interaction and Climate Variability,* C. Wang, S.-P. Xie, and J. A. Carton, Eds., Amer. Geophys. Union, 121–141.

Zebiak, S. E., 1993: Air-sea interaction in the equatorial Atlantic region. *J. Climate,* **6,** 1567–1586.

——, and M. A. Cane, 1987: A model El Nino–Southern Oscillation. *Mon. Wea. Rev.,* **115,** 2262–2278.

Zeng, N., J. D. Neelin, and C. Chiou, 2000: A quasi-equilibrium tropical circulation model-implementation and simulation. *J. Atmos. Sci.,* **57,** 1767–1796.